NATIONAL ADVISORY COMMITTEE FOR AERONAUTICS

TECHNICAL NOTE 3837

INVESTIGATION OF HEAT TRANSFER FROM A STATIONARY AND ROTATING ELLIPSOIDAL FOREBODY OF FINENESS RATIO 3

By James P. Lewis and Robert S. Ruggeri

Lewis Flight Propulsion Laboratory
Cleveland, Ohio

Washington
November 1956

NATIONAL ADVISORY COMMITTEE FOR AERONAUTICS

TECHNICAL NOTE 3837

INVESTIGATION OF HEAT TRANSFER FROM A STATIONARY AND ROTATING ELLIPSOIDAL FOREBODY OF FINENESS RATIO 3

By James P. Lewis and Robert S. Ruggeri

SUMMARY

The convective heat transfer from the surface of an ellipsoidal forebody of fineness ratio 3 and 20-inch maximum diameter was investigated in clear air for both stationary and rotating operation over a range of conditions including air speeds up to 240 knots, rotational speeds up to 1200 rpm, and angles of attack of 0°, 3°, and 6°. The results are presented in the form of heat-transfer coefficients and the correlation of Nusselt and Reynolds numbers. Both a uniform surface temperature and a uniform input heater density distribution were used.

The experimental results agree well with theoretical predictions for uniform surface temperature distribution. Complete agreement was not obtained with uniform input heat density in the laminar-flow region because of conduction effects. No significant effects of rotation were obtained over the range of airstream and rotational speeds investigated. Operation at angle of attack had only minor effects on the local heat transfer. Transition from laminar to turbulent heat transfer occurred over a wide range of Reynolds numbers. The location of transition depended primarily on surface roughness and pressure and temperature gradients. Limited transient heating data indicate that the variation of surface temperature with time followed closely an exponential relation.

INTRODUCTION

In the general field of design of modern all-weather aircraft, the problem of protecting bodies of revolution against icing has become of increasing importance. Many aircraft components are essentially simple bodies of revolution; examples of these are radomes, body noses, engine accessory housings, and the large spinners of turboprop engines. The design of thermal icing protection systems for these components requires knowledge of the heat-transfer relations for both stationary and rotating bodies of revolution. Such information is of interest also in the general field of heat transfer. Several theoretical studies of the problem have

been made (refs. 1 and 2). However, very little experimental heat-transfer data for such bodies are available and the data are generally of limited scope.

Experimental investigations have been made at the NACA Lewis laboratory of the heat transfer from bodies of revolution in order to obtain more extensive data than are presently available, including the effects of angle of attack and rotation. The investigation was made as part of a general study of icing and icing protection of bodies of revolution. This report presents the results of an investigation of the heat transfer in clear air from the surface of an ellipsoidal forebody of fineness ratio 3 and a 20-inch maximum diameter. Similar results for a larger-diameter ellipsoidal forebody of fineness ratio 2.5 are reported in reference 3. In the present study the steady-stage convective heat transfer was determined with and without rotation of the ellipsoidal forebody over a range of airspeeds up to 240 knots, rotational speeds up to 1200 rpm, and angles of attack of 0°, 3°, and 6°. Limited transient heating data were also obtained. Heat was provided by an internal electric heater designed and instrumented to yield as much basic heat-transfer data as possible while at the same time preserving the performance and constructional details of a representative practical heater installation.

SYMBOLS

A area across which heat is transferred, sq ft

c_p specific heat at constant pressure, Btu/(lb)($^{\circ}$F)

D_e maximum diameter of spinner (minor axis of ellipsoid), ft

D_w diameter of trip wire, ft

H convective heat-transfer coefficient, Btu/(hr)(sq ft)($^{\circ}$F)

K constant

k thermal conductivity of air, Btu/(hr)(sq ft)($^{\circ}$F/ft)

Nu_e body Nusselt number, HD_e/k_0

Nu_s local Nusselt number, Hs/k_a, dimensionless

n exponent

Pr Prandtl number based on free-stream stagnation air temperature properties, $\mu_a c_p/k_a$, dimensionless

Q total rate of heat input, Btu/hr

Q_{Al} rate of heat conduction between heater elements, through aluminum skin, Btu/hr

Q_i rate of heat flow to body interior, Btu/hr

Q_s rate of heat transfer from external surface, Btu/hr

Re_s local surface Reynolds number, $\frac{U_s W_a s}{\mu_a}$, dimensionless

Re_θ local boundary-layer Reynolds number, $\frac{U_s W_a \theta}{\mu_a}$, dimensionless

Re_0 free-stream Reynolds number, $\frac{U_0 W_0 D_e}{\mu_0}$, dimensionless

r local radius of ellipse, ft

s surface distance from nose, ft

T absolute temperature, $^{\circ}R$

t_d datum or unheated-surface temperature, $^{\circ}F$

t_h heater interior temperature as measured by thermocouple h (fig. 2), $^{\circ}F$

t_i inside temperature of heater insulation as measured by thermocouple i (fig. 2), $^{\circ}F$

t_s spinner surface temperature as measured by thermocouple s (fig. 2), $^{\circ}F$

t_0 free-stream static temperature, $^{\circ}F$

U_s local velocity on spinner surface, ft/sec

U_0 free-stream air velocity, ft/sec or knots

W specific weight of air, lb/cu ft

α angle of attack, deg

θ boundary-layer momentum thickness, ft

μ absolute viscosity of air, lb/ft-sec

τ heating or cooling time, sec

τ^* time constant, sec

Subscripts:

A,B,C, D,E,F, G,H heater elements (fig. 2)

Al aluminum skin

a stream stagnation condition

av value averaged over area of heater element

cr critical

max maximum

s surface condition

sp spinner stagnation point

0 free-stream static condition

APPARATUS

The model, consisting of half of an ellipsoidal body of revolution with a half major axis of 30 inches and a half minor axis of 10 inches, was mounted on a faired afterbody in the 6- by 9-foot test section of the Lewis icing research tunnel (fig. 1). The test model proper, consisting of the ellipsoidal forebody, is hereinafter referred to as the spinner model to distinguish it from the entire assembly. The afterbody, power-supply system, thermocouple pickup, and temperature recording system were essentially the same as used in the tests of reference 3. The spinner model was fabricated of 0.062-inch aluminum spun in one piece to the desired shape. An ogive transition section 15 inches long faired the contour between the rear of the 20-inch-diameter spinner and the 30-inch diameter afterbody. The rear of the spinner model was located at the same position relative to the afterbody as was the rear of the 30-inch-diameter spinner of reference 3. Heat was supplied to the spinner by electric heaters located on the inside surface of the spinner shell.

The spinner contour, heater layout, and details of the heater construction and thermocouple installation are shown in figure 2. The heater was divided into eight areas, each constituting a single circuit connected to separate autotransformers permitting selective control of heat density

and axial heat distribution. The heat input to each heater area was measured by a voltmeter and an ammeter. The spinner surface area for each heater is listed in table I. The longitudinal heaters (G and H) were located on two diametrically opposite sides of the spinner; these heaters were designed to provide parting areas for subsequent cyclic deicing tests.

The heating elements consisted of strands of 36-gage Nichrome heating wires encased between plies of glass cloth and silastic (silicone plastic). The higher temperature limit of the silicone compared with the neoprene insulation used in the heaters of reference 3 permitted operation at higher skin temperatures and heat densities. Copper-constantan thermocouples were installed at various locations to obtain both the skin temperature distribution and the inward heat dissipation. A sketch of the system used to transmit the temperatures from the thermocouples to the recorder is shown in figure 3(a). Details of the operation of this system are given in reference 4.

In order to evaluate the effects of surface roughness at the nose of the body on the heat transfer, a boundary-layer trip was cemented to the spinner surface for a few of the tests. The trip, consisting of a circular loop made of 0.01-inch-diameter wire, was located at a surface distance of 0.75 inch from the nose.

The pressure distribution over the spinner surface was obtained from pressure belts cemented to the spinner surface for stationary operation of the spinner. The belts consisted of 23 parallel plastic pressure tubes formed into a single strip. A hole was made in the side wall of each tube at the surface location for which pressure measurements were desired. The belts were attached to diametrically opposite sides of the spinner in the plane of angle of attack (tunnel horizontal plane). For spinner rotation, flush surface pressure taps and a rotating pneumatic pressure pickup were used. Details of the rotating pressure pickup are given in figure 3(b). Computations of the effect of centrifugal force on the pressure measurements indicated a maximum correction of 8 percent. No corrections were made to the data, however, because experimental checks showed only negligible effects of rotation.

PROCEDURE

Experimental Procedure

The pressure distribution was obtained at airspeeds of 152 to 240 knots, angles of attack of 0°, 3°, and 6°, and rotational speeds of 0, 800, and 1200 rpm. Rotation was in a clockwise direction looking upstream, and the angle of attack was directed to the left in a horizontal plane looking upstream.

Heat-transfer data were obtained primarily for steady-state heating. Two nominal heating conditions were used: (1) a uniform surface temperature distribution with nominal values of 100° and 200° F, and (2) a uniform input heat density to all heater elements with a nominal value of 10 watts per square inch. In addition, measurements of the unheated equilibrium model temperatures were taken for each condition in order to obtain reference temperatures used in the computation of the heat-transfer coefficient. The nominal operating conditions were airspeeds of 175 and 240 knots; rotational speeds of 0, 800, and 1200 rpm; angles of attack of 0°, 3°, and 6°; and an air total temperature of 0° F. These heating and operating conditions gave free-stream Reynolds numbers (Re_0) of 3.5×10^6 to 4.9×10^6 and skin to free-stream temperature ratios T_s/T_0 of 1.22 to 1.47.

In addition to steady-state heating, a limited study of transient heating was made. In these tests power of a predetermined density was applied to the model until the heated equilibrium surface temperature was obtained. The variation of spinner surface temperature with time at several surface positions was obtained during this heating period and in the subsequent cooling period. For these tests the heat input was that which gave a uniform surface temperature distribution in the steady state.

Method of Analysis

Experimental data. - The experimental results are presented in terms of the heated-surface temperature rise above the unheated-surface equilibrium temperature $t_s - t_d$, the external convective heat-transfer coefficient H, and the local Nusselt number Nu_s.

The convective heat-transfer coefficient was computed from the following relations:

$$H = \frac{Q_s}{A(t_s - t_d)}$$

$$Q_s = Q - Q_i \pm Q_{Al}$$

A sketch of the assumed heat flow from the heater is shown in figure 4. The heat dissipated to the inside of the heater Q_i was computed from

$$Q_i = 28.8\ A(t_h - t_i)$$

The effective thermal conductivity of 28.8 Btu/(hr)(sq ft)($^{\circ}$F) for the 0.060-inch insulating layer between the two inner thermocouples h and i (fig. 2) was obtained from tests of an instrumented sample of the heater. The maximum inward heat transfer was approximately 15 percent of the heat input; most of the inward heat transfer, however, was of the order of 5 percent of the heat input. The greatest inward heat transfer occurred at regions of steep temperature or heat-input gradients in the longitudinal direction.

The meridional or longitudinal heat conduction was approximated by assuming that all the conduction occurred within the aluminum skin. Referring to figure 4, Q_C is the measured heat input to heater segment C. The heat conducted between adjacent heater segments is

$$Q_{Al} = \pm k_{Al} A_{Al} \frac{dt_s}{ds}$$

The heat balance for a heater segment (e.g., heater C) is

$$Q_{s,C} = Q_C \pm Q_{Al,B-C} \pm Q_{Al,C-D} \pm Q_{i,C}$$

and similarly for the other heater segments. This conduction correction was applied only for the case of uniform heat input, where valid determinations of the surface temperature gradient dt_s/ds, were obtained. No accounting for circumferential conduction was made.

Most of the results are presented in terms of an average heat-transfer coefficient for each heater segment. This average coefficient was obtained from area-averaged values of surface temperature and external heat-flow rate. In addition, local effective coefficients were computed using local surface temperatures indicated by each thermocouple and a heat-flow rate defined as the heater-segment input density minus the local internal heat dissipation. This local heat-transfer coefficient is, of course, not a true coefficient, since the exact local heat dissipation from the external surface is not used. The local effective coefficients so defined are the heat-transfer coefficients reported in reference 3 and, in addition, are of interest as indicating the surface temperature behavior for installations having similar heater construction and heat distribution.

For uniform surface temperature, the longitudinal heater elements G and H (fig. 2) were set at a heat density approximating that of adjacent circumferential heaters. The effective heat-input density Q/A for this case was taken as an area-weighted average of the heat densities on adjacent circumferential and longitudinal heaters at each surface distance location from the nose.

The Nusselt, Reynolds, and Prandtl numbers used in the correlation of the experimental data are defined as follows:

$$Nu_s = Hs/k_a$$

$$Re_s = \frac{U_s s}{\mu_a} W_a$$

$$Pr = \frac{\mu_a c_p}{k_a}$$

In all these parameters the air properties were evaluated at the free-stream stagnation temperature for simplicity in calculating. As indicated in reference 3, the correlation of the results, for the temperature range of interest, is affected only slightly by the choice of the specific temperature at which the air properties are evaluated.

When the average heat-transfer coefficients were used, it was necessary to determine a corresponding surface distance for the calculation of the average Nusselt and Reynolds numbers. This average distance was determined as follows. From theoretical analyses the local convective heat-transfer coefficient can be expressed as a function of the surface distance in the form

$$H = Ks^n \tag{1}$$

where the values of the constant K and the exponent n depend upon whether laminar or turbulent heat transfer is being considered. It is assumed that the average coefficient H_{av} follows the theoretical variation with the average surface distance s_{av}; that is,

$$H_{av} = K(s_{av})^n \tag{2}$$

The average coefficient over the area between the cumulative areas A_1 and A_2 can be expressed as

$$H_{av} = \frac{\int_{A_1}^{A_2} H \, dA}{A_2 - A_1} \tag{3}$$

Substituting for the local coefficient from equation (1) and the relation between dA and dS, equation (3) becomes

$$H_{av} = \frac{2\pi K \int_{s_1}^{s_2} r s^n \, ds}{2\pi \int_{s_1}^{s_2} r \, ds} \tag{4}$$

The relation between the local radius of the ellipse r and s being known, equations (2) and (4) may be set equal and solved for s_{av} in terms of s_1 and s_2. The distance s_{av} differed significantly from an arithmetic mean of s_1 and s_2 only near the nose. In the transition region where the theoretical variation of H with s is unknown, an arithmetic mean of s_1 and s_2 was used.

The transient temperature data are presented in terms of the heated-surface temperature rise above the equilibrium unheated-surface temperature $t_s - t_d$. The transient results are also presented in terms of the time constant τ^*, which is defined as the time required for the surface temperature to reach $1 - (1/e)$, or 63.2 percent of the asymptotic temperature change.

Theoretical heat transfer. - The experimental heat-transfer results are compared with the predicted values of several theoretical analyses. For the laminar boundary layer in steady-state heating, the predicted heat transfer was obtained from the method of Squire as computed in reference 1 and by the method of Drake (ref. 2). The analysis of Squire is for a uniform surface temperature only, while Drake's method yields results for arbitrary surface temperature and heating-rate distributions. Calculations with the Drake method were made for both uniform surface temperature and uniform surface heating rate.

The predicted heat-transfer relation of Squire for the stagnation region obtained from reference 1 for uniform surface temperature is

$$Nu_e = 0.681 \sqrt{\left[\frac{d\left(\frac{U_s}{U_0}\right)}{d\left(\frac{s}{D_e}\right)}\right]_{sp}} \, Re_0$$

Drake's method (ref. 2) yields a similar relation, with the value of the constant equal to 0.665 for uniform surface temperature and 0.816 for uniform heating rate. These constants are for a Prandtl number of 0.72.

For the turbulent boundary layer, the method of Squire was also employed in addition to the modified flat-plate turbulent heat-transfer equation of Martinelli given in reference 5 as

$$Nu_s = (Pr)^{1/3}\, 0.0296(Re_s)^{0.8}$$

RESULTS AND DISCUSSION

Velocity Distribution

The local velocity over the spinner surface is required in the correlation of the heat-transfer data. In addition, a comparison of the measured velocity distribution with theoretical values indicates the magnitude of any tunnel effects and, hence, the validity of the tunnel simulation. The ratio of the local velocity to the free-stream velocity is presented in figure 5. These data are uncorrected for tunnel effects, because this measured value is that which is required for the correlation of the heat-transfer results. A theoretical curve obtained by the method of reference 6 for nonviscous incompressible flow is also presented in figure 5(a) for an angle of attack of 0°.

The experimental data over most of the spinner surface agree well with the theoretical curve. Practically no variation of the velocity ratio with free-stream Reynolds number was obtained; the values plotted in figure 5(a) are an average for the Reynolds number range investigated. Some scatter of the data near the nose made the determination of the location of the air stagnation point somewhat inexact. In the nose region, however, the slope of the experimental velocity-ratio curve (used in predicting the heat-transfer coefficient) agrees with the theoretical value within the limits of experimental accuracy. At stagnation, the value of the slope of the velocity gradient $\left[d(U_s/U_0)/d(s/D_e)\right]$ was taken as 7.6 for 0° angle of attack in the calculation of the theoretical heat transfer.

The local velocity distribution for the rotating spinner is compared with the results for the stationary spinner in figure 5(b) at an angle of attack of 0°. No significant effect of rotation on the local velocity was obtained even at the maximum rotational speed (1200 rpm). This result might be expected, since the local velocities for the stationary spinner are only 5 percent less, at the most, than the local velocities computed as the resultants of the longitudinal and rotating components. Because of the slow time response of the pressure-sensing system, the local velocities for the rotating case at angle of attack were a time-average of the upper- and lower-surface values obtained at the stationary condition.

Steady-State Heat-Transfer Results

The steady-state heat-transfer results are discussed first in terms of a general correlation of the results for the separate cases of uniform surface temperature and uniform input power density, and secondly in relation to the specific effect of the several operating variables.

Uniform surface temperature. - Typical results obtained with a uniform surface temperature are shown in figure 6. The surface temperature rise, $t_s - t_d$, heater input power density, and convective heat-transfer coefficient are given for the stationary spinner at 0° angle of attack. (The measured unheated equilibrium surface temperature was essentially constant over the body surface for all tests.) The data of figure 6 were obtained with the spinner surface in its smoothest condition. The segment average coefficient is shown by the stepped straight lines, while the data points are the local effective coefficients. The experimental heat-transfer coefficients agree well with the theoretical stagnation, laminar, and turbulent values. A fairly extensive region of laminar flow was obtained, with transition starting approximately 13 inches from the nose and a fully turbulent condition reached at approximately 24 inches from the nose. Included in figure 6 is the value of the lower critical Reynolds number of boundary-layer stability calculated from the analysis of Schlichting. For values less than the critical the boundary layer is assumed stable, and transition does not occur in the absence of surface roughness or other disturbing effects. Transition and boundary-layer stability are discussed later. Both the surface temperatures and heat-transfer coefficients reflect the unfaired stepped heat distribution.

The heat-transfer results of figure 6 are shown in the Nusselt, Prandtl, and Reynolds number form in figure 7. In terms of the local Reynolds number Re_s, transition began at approximately 2.3×10^6 and was completed at approximately 4.2×10^6. Fairing of a smooth curve through the heat-rate distribution would reduce the spread of the data to approximately 10 percent, and the experimental data would vary less than 10 percent from the theoretical values.

The heat transfer at several angles of attack and rotational speeds for the spinner with a uniform surface temperature is compared in figure 8. The results of several repeat runs made with the stationary spinner at 0° angle of attack (fig. 8(a)) indicate good reproducibility of data and agree well with the theoretical values. These data are similar to those obtained at a lower stream Reynolds number (fig. 7), except that the local Reynolds number of transition is lower in figure 8(a). This forward movement of transition is attributed to the increased surface roughness in the region of rapidly decreasing velocity gradient ($s > 5$ in.) rather than the increased stream Reynolds number or stream turbulence. During the progress of the tests the entire surface gradually became

roughened by foreign particles in the tunnel airstream, although the spinner surface was hand-sanded lightly at intervals throughout the course of the investigation in an effort to keep the degree of surface roughness fairly constant.

While the spinner surface was still relatively smooth (same condition as for fig. 6), a wire boundary-layer trip was installed near the nose of the spinner in order to determine the effects of surface roughness at the nose area on heat-transfer results. No significant effect of the trip was obtained; the experimental data points fell almost exactly on those obtained without the trip (fig. 6). The absence of any effect of the trip on transition is attributed to the favorable pressure gradient at the trip location; any disturbing effect of the trip was apparently immediately dampened before transition to turbulent flow can occur. Transition effects are discussed in more detail in a later section. The data of figures 7 and 8 show the extreme range of location of transition for the uniform surface temperature extending from Re_s of approximately 10^6 to approximately 5×10^6.

The Nusselt and Reynolds numbers for the rotating spinner at angle of attack (figs. 8(b) and (c)) are based upon a surface distance computed vectorially from a helical path associated with the rotational speed. Good agreement with the theoretical values for angles of attack of 3° and 6° was obtained, as for the stationary spinner at 0° angle of attack, and transition occurred over approximately the same Reynolds number range. There was no increase in Nusselt number with rotational speed. This result would be expected because of the minor effects of rotation on the local surface velocity.

Uniform heat input. - Typical results obtained with an essentially uniform input heat density are given in figure 9. These results were obtained concurrently with those of figures 6 and 7 (uniform surface temperature) with the smoothest skin condition. A theoretical curve, computed by the method of reference 2, for laminar heat transfer with a uniform heating rate is given in addition to that for a uniform surface temperature. This predicted curve assumes a uniform rate of heating at the spinner external surface, while in the experiments a uniform heat input to the heaters was used. The average heat-transfer coefficient corrected for longitudinal conduction is shown in figure 9 as stepped straight lines, while the data points are the uncorrected effective local values. The corrected average heat-transfer coefficients agree well with the theoretical values for a uniform surface temperature over the first 6 inches of surface, followed by a long transition region with turbulent values being approached at the rear of the spinner.

The heat-transfer results of figure 9 are replotted in the form of Nusselt, Prandtl, and Reynolds numbers in figure 10. Comparison of the corrected average and effective local data points indicates that significant conduction effects occurred only over the first two heaters (A and B). The transition region extends over a greater Reynolds number range than for the case of uniform surface temperature.

The effects of variations in the free-stream velocity, angle of attack, and rotational speed on the correlation of the heat transfer with a uniform input heat density are presented in figure 11. The correlation parameters are defined in terms of the corrected average values, the helical path for the case of rotation, and the surface distance from stagnation point for angle of attack. The results are similar to those of figure 10. No significant or systematic effects with changes in free-stream velocity, angle of attack, or rotational speed were obtained except in the transition region, and those were probably caused by variations in surface roughness. The experimental results in the laminar region fall between the two theoretical curves for uniform heating rate and uniform temperature. The failure of the experimental results to follow the theoretical curve for a uniform heating rate may be attributed to the fact that conditions of surface temperature and heating-rate distribution assumed in the derivation of the theoretical relation do not correspond to the conditions actually found to exist on the spinner surface. These differences probably result from conduction effects, pressure and temperature gradients, effects of transition, and approximations inherent in the theoretical development. In general, the heat-transfer results obtained with a uniform input heat density exhibit the same trends as those of reference 3 for similar heating conditions.

Effect of operating variables on heat transfer. - In order to illustrate the effects of free-stream velocity, angle of attack, and rotational speed on the heat transfer, the surface temperature and heat-transfer coefficient are presented for specific conditions as a function of the surface distance from the spinner nose. The changes in heat transfer at two free-stream velocities and two uniform surface temperatures for the stationary spinner at 0° angle of attack are shown in figure 12(a). The major differences in the heat-transfer coefficient are the result of the change in stream velocity rather than the surface temperature change. Both the laminar and turbulent heat-transfer coefficients increase with an increase in stream velocity, following closely the theoretically predicted increase with change in velocity. Theoretical considerations indicate that an increase in surface temperature would tend to increase the heat-transfer coefficient and cause a forward movement of transition. The experimental results, however, show the opposite trend. In addition, an increase in stream velocity moved the location of transition forward, as expected from theory; at the higher speed, transition was initiated at approximately 5 inches from the nose, compared with approximately 8 inches at the lower velocity. In both cases transition started forward

of the location of lower critical stability Reynolds number. Transition was completed approximately 17 inches from the nose for both stream velocities.

For the case of uniform heat input density, similar variations in the heat-transfer coefficient were obtained, as shown in figure 12(b). The increase in the laminar and turbulent heat-transfer coefficients with velocity followed closely the theoretical predictions. The corresponding decrease of surface temperature with the increased stream velocity is also shown in figure 12(b). Surface temperature changes as large as 150° F were obtained, together with a forward shift of the position of the peak temperature from 9 inches to 4 inches from the nose. This shift of the peak temperature is indicative of a movement of transition over approximately the same range.

The surface temperature distribution and heat-transfer coefficients obtained at two angles of attack are compared in figure 13 for the stationary spinner with a uniform heat input density. The results in figure 13(a) are for two diametrically opposite meridional locations in the plane of angle of attack. The influence of angle of attack on the heat transfer was minor, being primarily a shift of the stagnation and transition regions towards the windward side. Additional data at 6° angle of attack are shown in figure 13(b) for three meridional locations. The effects on transition are similar to those of figure 13(a), the transition curve shifting forward with increasing meridional angle location but with very little change in the shape of the curve. The data obtained at the 90° meridional location at 6° angle of attack were much the same as those obtained at 0° angle of attack.

The variation of the heat-transfer coefficient with rotational speed for three angles of attack is given in figure 14 for a uniform surface temperature distribution. Rotational speeds as high as 1200 rpm had a negligible effect, the heat-transfer coefficient varying less than 10 percent. Similar results were obtained with a uniform input heat distribution. These results are in accordance with the data of figure 5, which shows no significant effect of rotation on the local surface velocity.

Comparison with 30-inch-diameter spinner (2.5 fineness ratio). - Some of the results of the present investigation are compared in figure 15 with typical data from the investigation of heat transfer from a 30-inch-diameter ellipsoidal spinner of 2.5 fineness ratio (ref. 3). For the stationary case (fig. 15(a)) the results for the two spinners agree fairly well, except for the region near the nose. This discrepancy resulted from the fact that no conduction corrections were applied to the data for the 30-inch-diameter spinner. The spread of the data for the 30-inch spinner in the transition region is attributed to variations in surface roughness rather than to the differences in heat density.

At a rotational speed of 1200 rpm (fig. 15(b)), the larger spinner gave considerably larger heat-transfer coefficients in the transition and turbulent regions. This effect is believed to be caused primarily by the larger radius of the 30-inch spinner, giving a proportionately larger effect of the rotating velocity component. In addition, differences in heater construction of the two spinners may have led to differences in heat-conduction effects. A comparison of the heat-transfer results for the two spinners in the form of Nusselt and Reynolds numbers also yielded good agreement with the respective theoretical values, except for variations of the transition-region location.

Transition region. - In addition to the determination of the laminar and turbulent heat-transfer coefficients, knowledge as to the location and form of the transition region is required. At present, no general method of quantitatively predicting the location of transition is available. It is known that transition location depends upon stream turbulence, Mach number, surface temperature and curvature, surface temperature and pressure gradients, and surface roughness. Quantitative information as to the effects of these variables is very limited even for subsonic flow; this is especially true for the action of combined effects. Several empirical correlations of the effects of the several variables on transition have been proposed (refs. 7 and 8), which together with calculations of the boundary-layer stability provide a means of estimating the approximate location of transition for specific cases.

The experimentally determined transition regions for the stationary spinner with a uniform surface temperature distribution are presented in figure 16 in terms of the local boundary-layer Reynolds number Re_θ. The variation of Re_θ with surface distance from the spinner nose is shown by the dotted lines for each free-stream Reynolds number, with superimposed solid lines denoting the location of transition for each case. The boundary-layer Reynolds number was computed by the method of reference 2. Included for comparison is a curve of the lower critical boundary-layer Reynolds number, below which the boundary layer is assumed to be stable. The curve of $Re_{\theta,cr}$ is based on the calculations of Schlichting as presented in reference 9 applied to three-dimensional bodies.

Considering first the case of the smoothest surface condition ($Re_0 = 3\times10^6$), transition occurred in the unstable region at a value of Re_θ only slightly greater than the critical. While the stability criteria alone do not predict the location of transition, experimental data for a flat plate (ref. 8) and elliptic cylinders (ref. 10) show that, in the absence of surface roughness, transition approaches the stability limit as the stream turbulence intensity is increased. Previous heat-transfer data (ref. 11) and sphere drag measurements have indicated a fairly high turbulence level in the Lewis icing tunnel. As previously indicated, the installation of

a trip at the spinner nose had no measurable effect on transition. At the trip location, even though the trip is 9 times the momentum thickness of the boundary layer, the boundary layer is very stable (the critical boundary-layer Reynolds number is approximately 45 times the actual boundary-layer Reynolds number). It would appear that any effect of the presence of the trip is immediately dampened, and transition develops as before, primarily as a result of stream turbulence.

For other cases ($Re_0 = 3.6\times10^6$ and 5×10^6), in which a distributed roughness was known to exist on the spinner surface, transition occurred at values of Re_θ less than the critical value. It is believed that both the location and type of the roughness cause this result. For all the experimental work the most forward position of transition was at 3 to 4 inches from the nose. Figure 5 shows that forward of this location is a region of a very steep negative pressure gradient, which probably prevented forward movement of transition.

The experimental data showed no significant effect of rotation on the location of transition. This result might be expected because of the relatively small value of the rotational velocity component, which would minimize any boundary-layer twisting shear or centrifugal effects. The effect of angle of attack was only to shift the position of transition in accordance with the corresponding shift in the stagnation point and local velocity.

The variation of Reynolds number at the end of transition exhibited the same general trends as that at the initiation of transition but with a generally smaller variation. With the exception of a few points for uniform heat input, the end of transition occurred at local surface Reynolds numbers Re_s of approximately 3×10^6 to 5×10^6 as compared with a variation of approximately 0.8×10^6 to 2.3×10^6 for the beginning of transition. In general, the experimental results indicate that location of transition depends primarily on surface roughness effects and pressure and temperature gradients.

Transient Heating Results

Temperature-time histories of several points on the spinner surface are presented in figure 17 for both the heating and cooling periods for the stationary spinner at 0° angle of attack. These data were obtained with the heat distribution required for a steady-state uniform surface temperature distribution. Included in figure 17 are the experimentally determined time constants for five thermocouple positions. Additional time constants for both the heating and cooling periods are given in table II.

The temperature-time curves and the values of the time constants indicate that the heater installation had a relatively slow response. This fact is a result of necessary design and constructional features, including the electrical insulation between the heater wires and the spinner skin and the thermal insulation (with the corresponding large thermal capacity) on the heater inside surface required to reduce steady-state heat losses to the interior. The temperature response obtained is considered to be fairly good for the particular type of heater installation; any significant increase in the rate of response would require a radically different type of design and construction.

The surface temperature variation with time is shown in dimensionless form in figure 18 for typical surface locations. Included for comparative purposes are exponential curves of the form $\left(1 - e^{-\tau/\tau^*}\right)$ and $\left(e^{-\tau/\tau^*}\right)$ for the heating and cooling periods, respectively. The experimental surface temperature ratio follows closely the exponential variation with time, especially during the cooling period. From the definition of the time constant and the fact that the experimental temperature-time variation is essentially exponential, it appears that the temperature-time response at other operating conditions may be taken with sufficient accuracy as inversely proportional to the corresponding change in the heat-transfer coefficient.

SUMMARY OF RESULTS

From a study of the convective heat transfer from an ellipsoidal forebody of fineness ratio 3 in clear air, the following results were obtained:

1. The experimental heat-transfer coefficients for the case of a uniform surface temperature agreed well with the theoretical predictions of Drake, Squire, and Martinelli for the stagnation, laminar, and turbulent heat-transfer regions. Complete agreement in the laminar-flow region for the case of uniform input heat density was not obtained because of conduction effects.

2. Good correlation of the experimental results for all operating conditions was obtained by the use of the Nusselt-Prandtl-Reynolds number relation. No significant effects of rotation on the heat-transfer coefficients or transition were obtained for the range of rotational and airstream speeds investigated. Operation of the spinner at angles of attack up to 6° had only minor effects on the heat transfer, primarily causing a movement of transition in accordance with changes in the local velocity distributions. The time-averaged heat-transfer coefficients obtained at angle of attack with rotation of the spinner were essentially the same as obtained at 0° angle for the stationary spinner.

3. The heat-transfer results for the stationary spinner agreed well with those obtained with a 30-inch-diameter fineness ratio 2.5 spinner.

4. Transition from laminar to turbulent heat transfer occurred over a wide Reynolds number range, including both the movement of beginning of transition and also the extent of the transition region. The beginning of transition varied from a local surface Reynolds number of approximately 0.8×10^6 to 2.3×10^6 (corresponding to a boundary-layer Reynolds number between 200 and 600), depending upon surface roughness and pressure and temperature gradients. Beginning of transition did not occur forward of 3 to 4 inches from the nose. The end of transition varied over a local surface Reynolds number range of approximately 3×10^6 to 5×10^6. The effects of rotation and angle of attack on transition Reynolds number were negligible.

5. Transient heating data were obtained which indicated that the variation of surface temperature with time was essentially an exponential relation. The relatively large thermal capacity of the heater-spinner configuration caused a large temperature-time lag, as indicated by external surface time constants of approximately 50 to 80 seconds for both heating and cooling.

Lewis Flight Propulsion Laboratory
National Advisory Committee for Aeronautics
Cleveland, Ohio, August 6, 1956

REFERENCES

1. Torgeson, W. L., and Abramson, A. E.: A Study of Heat Requirements for Anti-Icing Radome Shapes with Dry and Wet Surfaces. WADC Tech. Rep. 53-284, Wright Air Dev. Center, Wright-Patterson Air Force Base, Sept. 1953. (Contract AF 33(616)-85, RDO No. 664-802.)

2. Drake, Robert M., Jr.: Calculation Method for Three-Dimensional Rotationally Symmetrical Laminar Boundary Layers with Arbitrary Free-Stream Velocity and Arbitrary Wall-Temperature Variation. Jour. Aero. Sci., vol. 20, no. 5, May 1953, pp. 309-316.

3. von Glahn, U.: Preliminary Results of Heat Transfer from a Stationary and Rotating Ellipsoidal Spinner. NACA RM E53F02, 1953.

4. Tarr, Philip R.: Methods for Connection to Revolving Thermocouples. NACA RM E50J23a, 1951.

5. Boelter, L. M. K., Grossman, L. M., Martinelli, R. C., and Morrin, E. H.: An Investigation of Aircraft Heaters. XXIX - Comparison of Several Methods of Calculating Heat Losses from Airfoils. NACA TN 1453, 1948.

6. Zahm, A. F.: Flow and Drag Formulas for Simple Quadrics. NACA Rep. 253, 1927.

7. Dryden, Hugh L.: Review of Published Data on the Effect of Roughness on Transition from Laminar to Turbulent Flow. Jour. Aero. Sci., vol. 20, no. 7, July 1953, pp. 477-482.

8. Gazley, Carl, Jr.: Boundary-Layer Stability and Transition in Subsonic and Supersonic Flow. Jour. Aero. Sci., vol. 20, no. 1, Jan. 1953, pp. 19-28.

9. Seban, R. A.: Calculation Method for Two-Dimensional Laminar Boundary Layers with Arbitrary Free Stream Velocity Variation and Arbitrary Wall Temperature Variation. Dept. Eng., ser. 2, no. 12, Univ. Calif., May 15, 1950. (A.T.I. No. 112297.)

10. Drake, R. M., Jr., Seban, R. A., Doughty, D. L., and Levy, S.: Local Heat-Transfer Coefficients on Surface of an Elliptical Cylinder, Axis Ratio 1:3, in a High-Speed Air Stream. Trans. A.S.M.E., vol. 75, no. 7, Oct. 1953, pp. 1291-1301; discussion, pp. 1301-1302.

11. Gelder, Thomas F., and Lewis, James P.: Comparison of Heat Transfer from Airfoil in Natural and Simulated Icing Conditions. NACA TN 2480, 1951.

TABLE I. - SPINNER HEATER DIMENSIONS

Heater	Surface distance from nose, s, in.	Heater surface area, sq in.
A	0 – 2	13.4
B	2 – 5	52.4
C	5 – 9	123
D	9 – 15	253.5
E	15 – 23	416
F	23 – 31.5	505.4
G	2 – 15	27
H	15 – 31.5	34.7

TABLE II. - TIME CONSTANTS

Surface distance from nose, s, in.	Time constant, τ^*, sec	
	Heating period	Cooling period
0	69	70
.45	70	67
1.00	66	69
1.50	74	77
2.25	72	77
2.55	76	81
3.10	80	83
3.5	86	79
4.00	81	82
5.15	87	81
6.15	80	73
7.10	79	74
8.20	60	53
9.35	63	57
10.55	77	66
12.00	57	50

Figure 1. - Installation of 20-inch-diameter (fineness ratio 3) elliptical spinner in icing research tunnel.

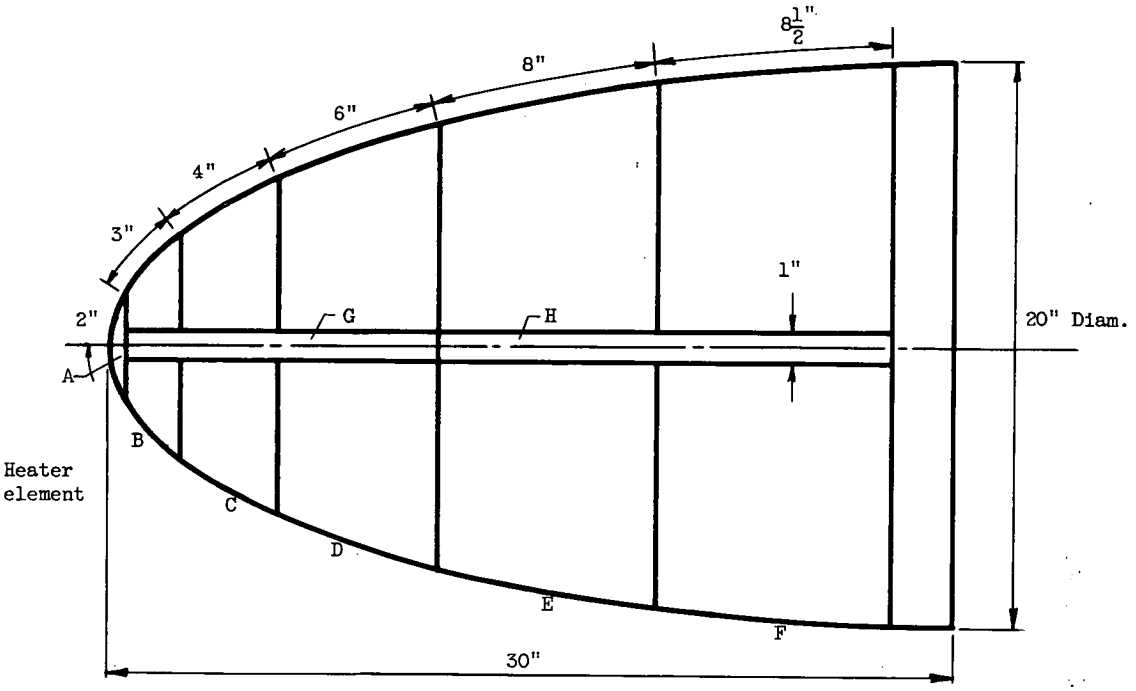

Heater layout

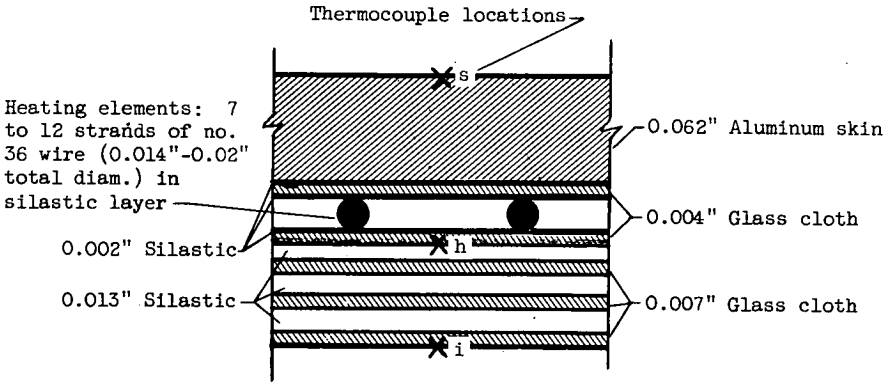

Section through heater

Figure 2. - Spinner contour and heater details.

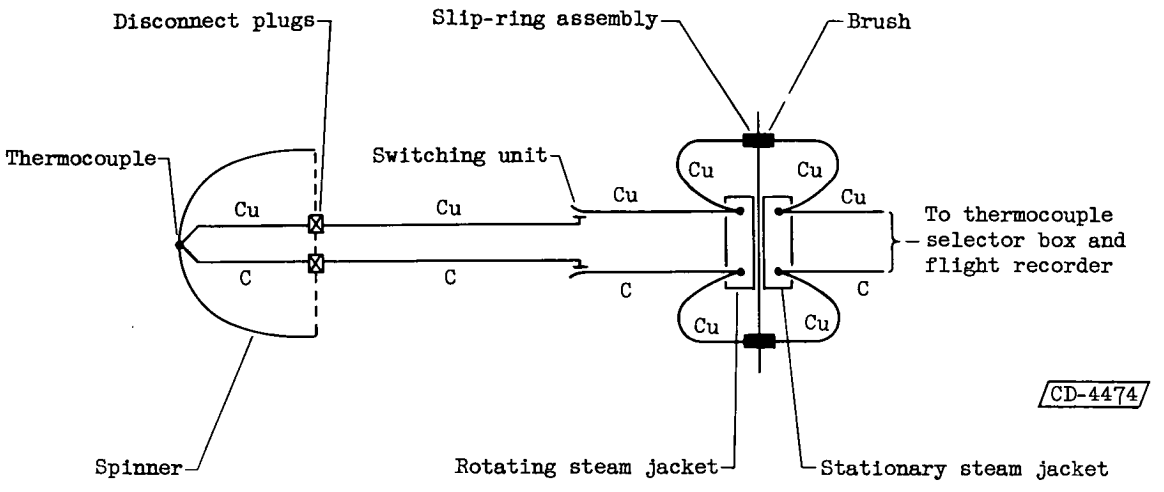

(a) Temperature-measuring system.

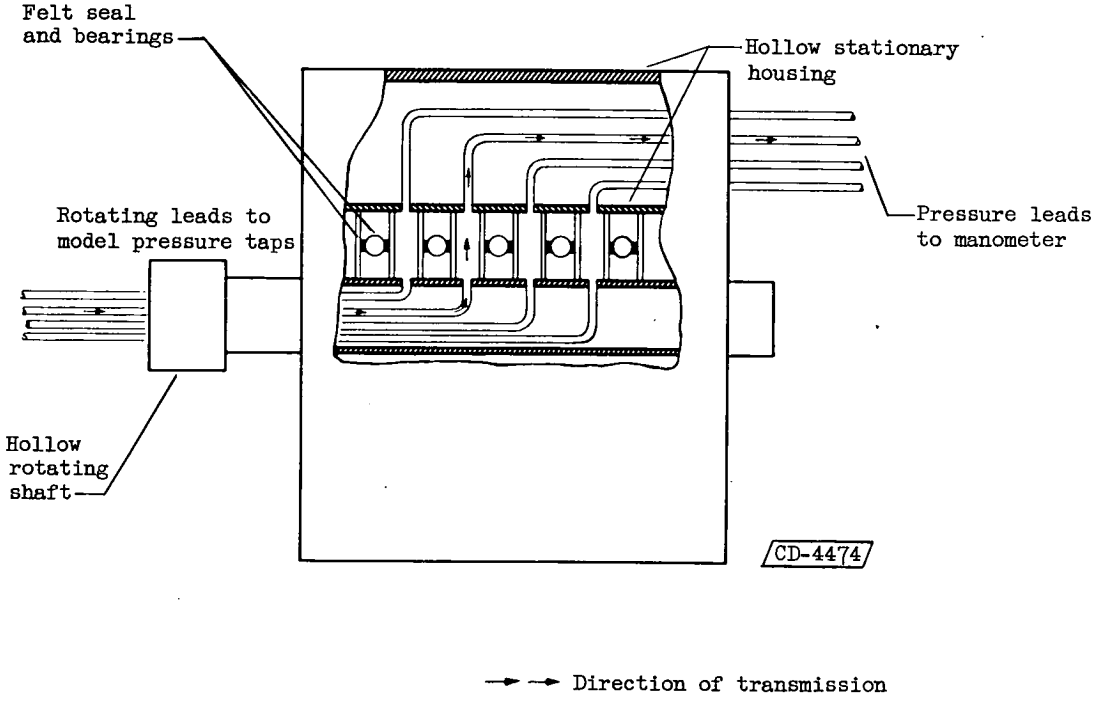

(b) Pressure-measuring system.

Figure 3. - Details of temperature- and pressure-measuring systems on rotating bodies.

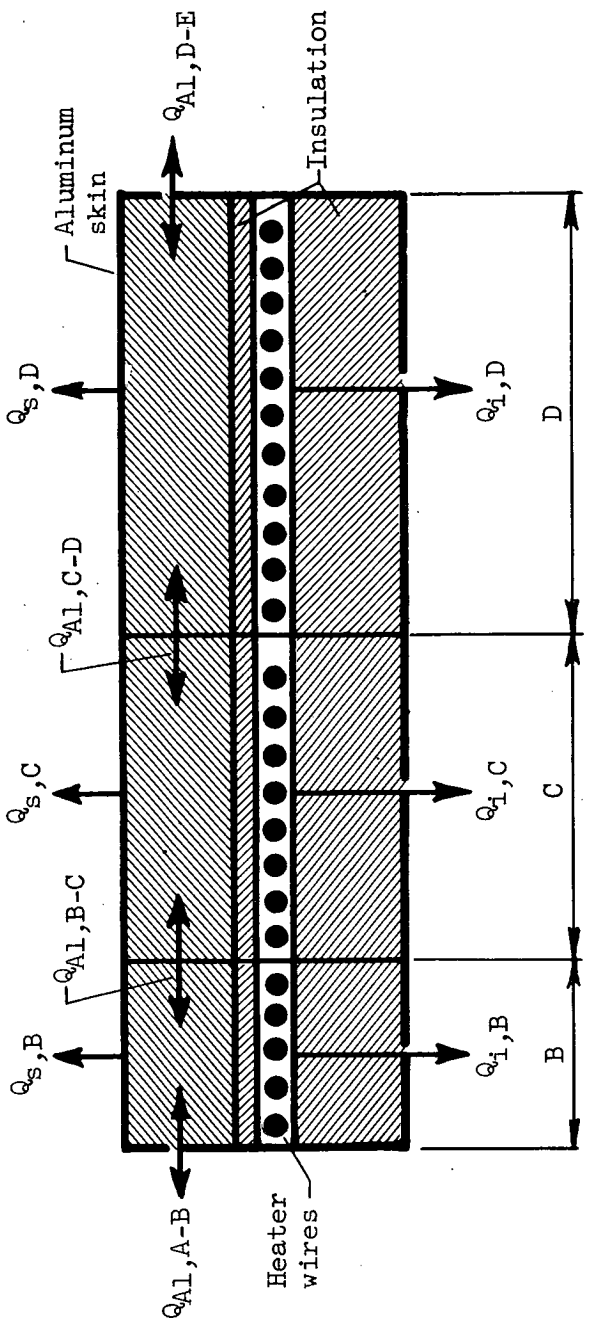

Figure 4. - Sketch of simplified heat-conduction path used in calculating external heat-transfer coefficients.

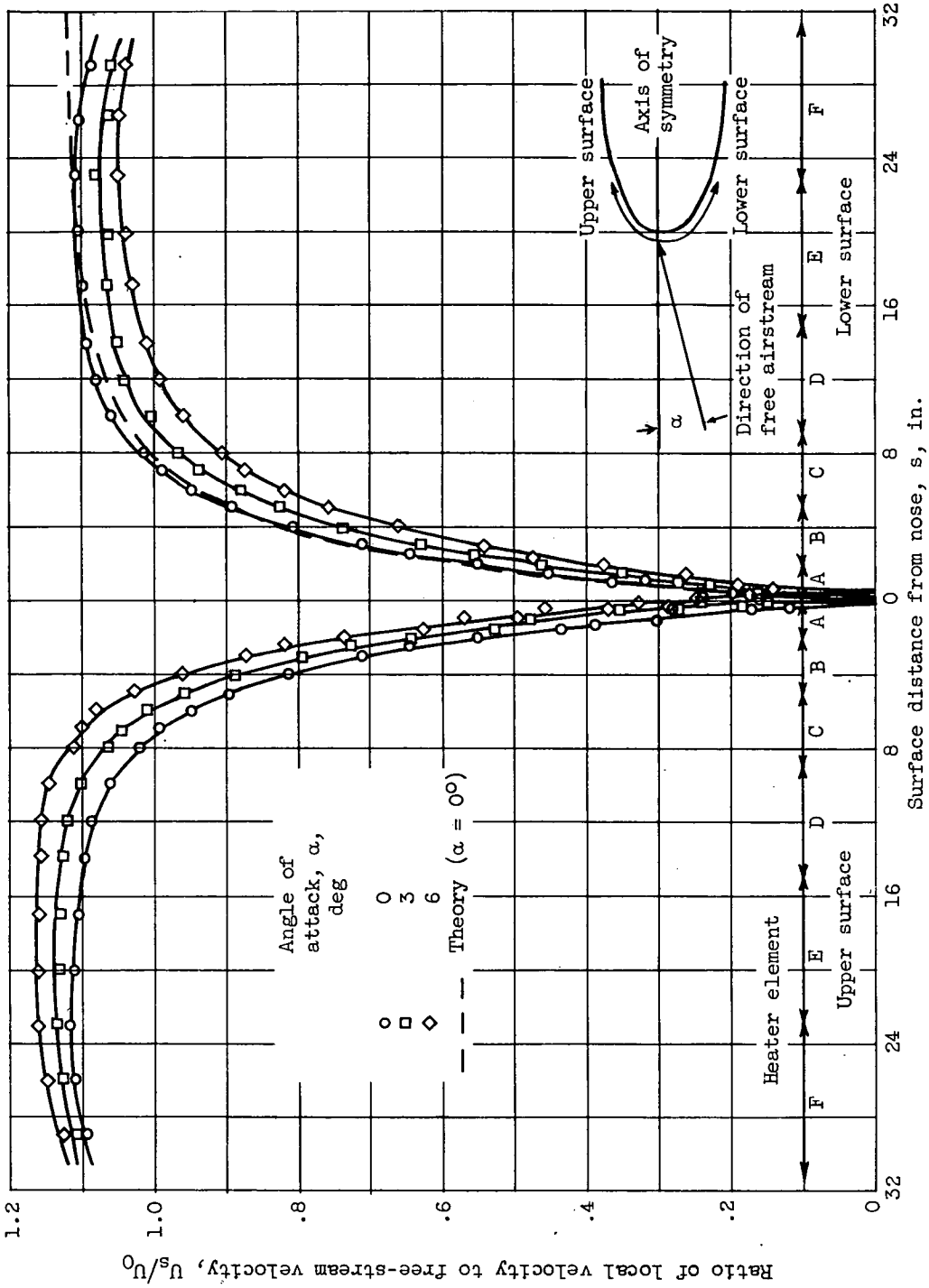

(a) Stationary spinner at three angles of attack. Free-stream Reynolds number, 4.2×10^6.

Figure 5. - Velocity distribution over spinner.

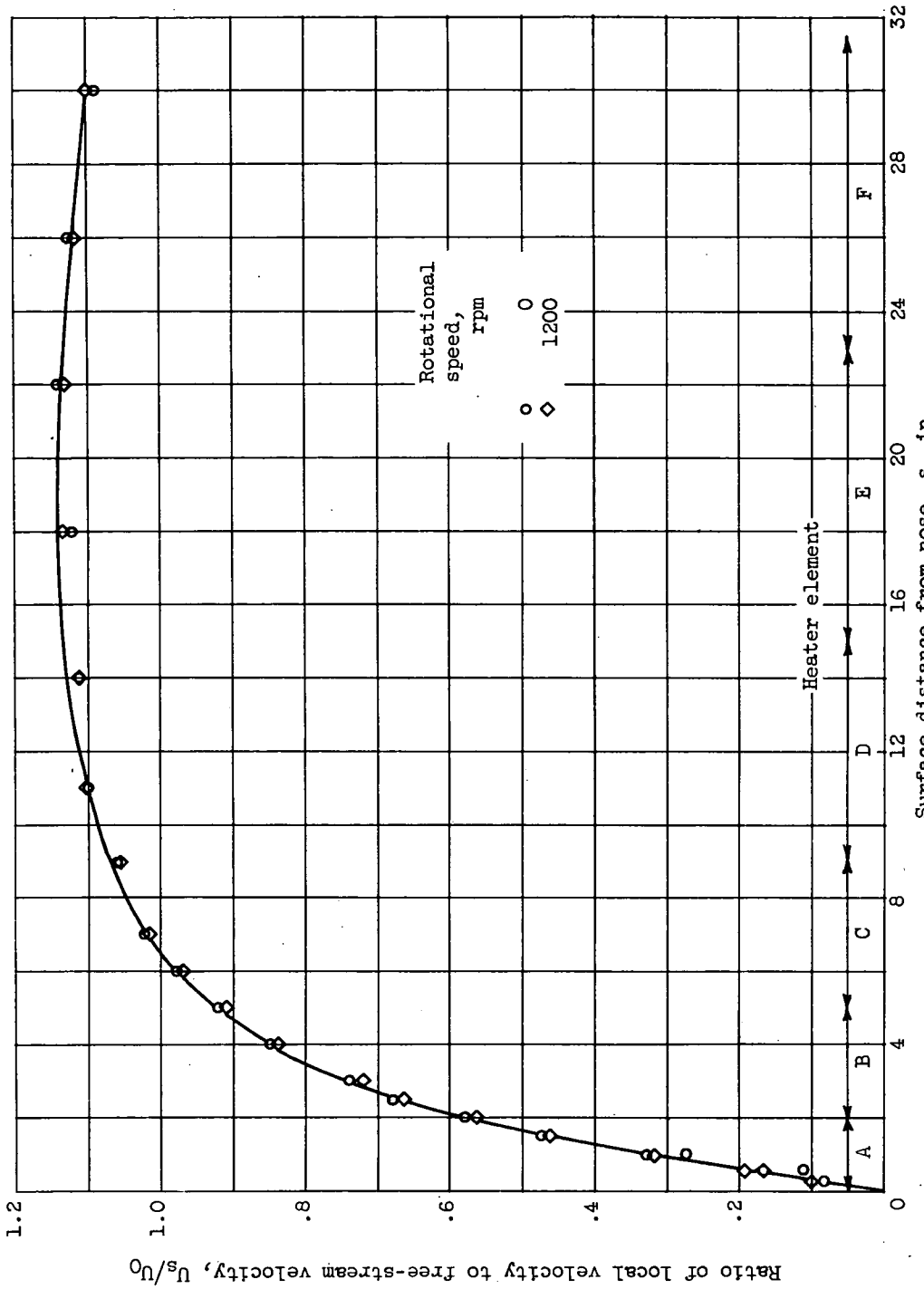

(b) Rotating spinner. Free-stream Reynolds number, 2.7×10^6; angle of attack, 0°.

Figure 5. - Concluded. Velocity distribution over spinner.

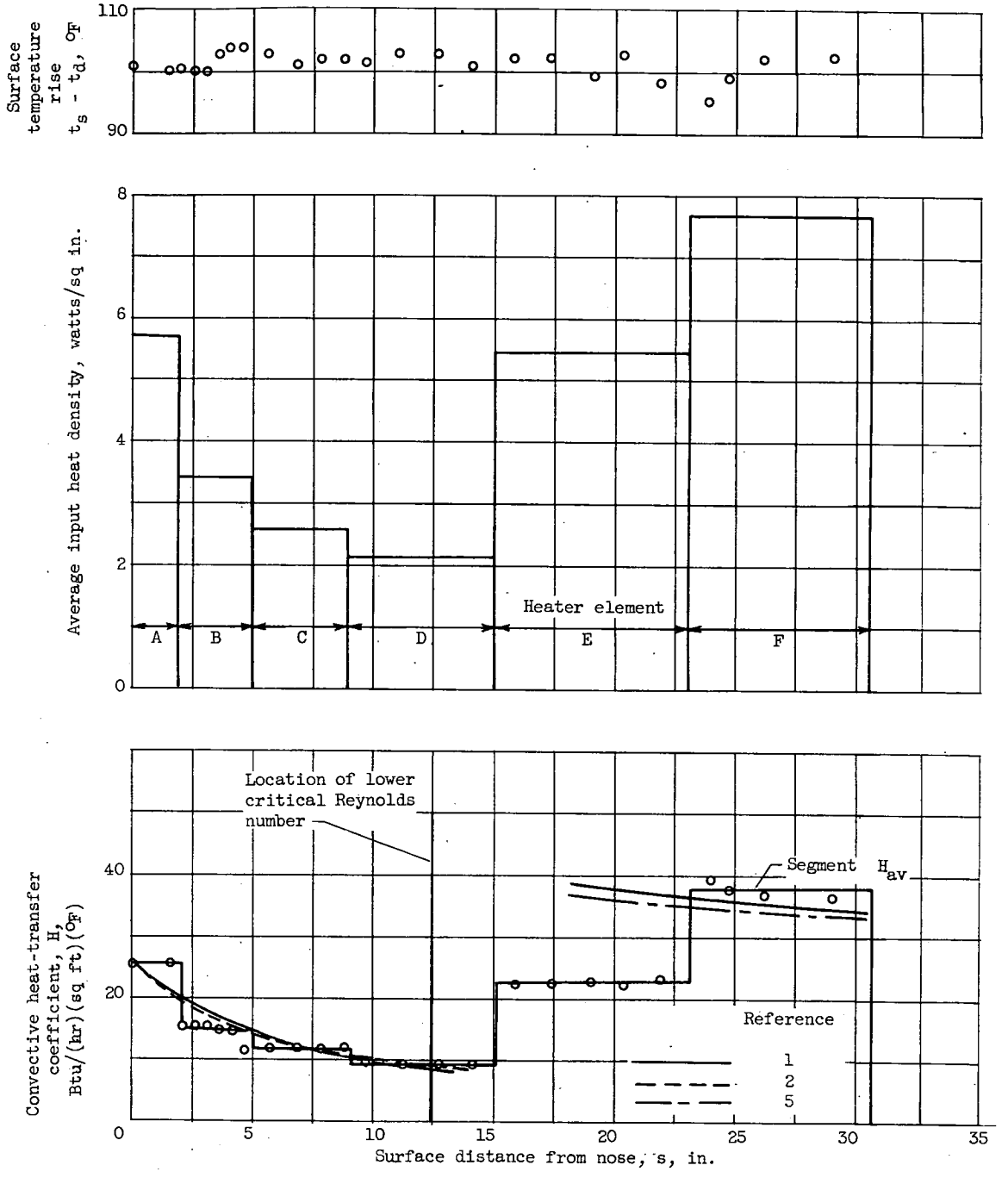

Figure 6. - Distribution of surface temperature, heat input, and convective heat-transfer coefficient for stationary spinner with uniform surface temperature. Free-stream velocity, 152 knots; air total temperature, 0° F; angle of attack, 0°.

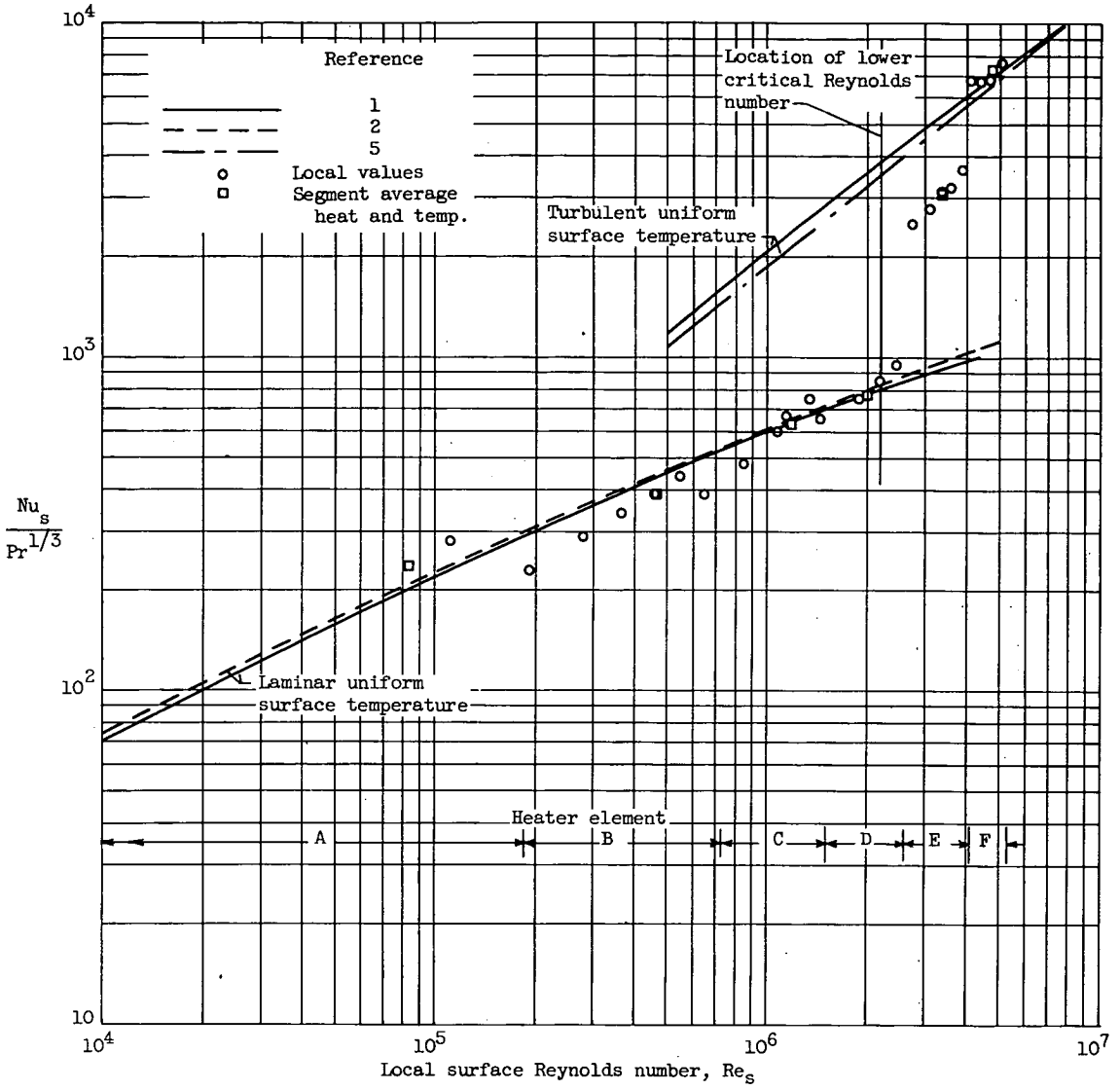

Figure 7. - Correlation of experimental and theoretical heat transfer for stationary spinner having uniform surface temperature of 100° F. Free-stream velocity, 152 knots; air total temperature, 0° F; angle of attack 0°; free-stream Reynolds number, 3×10^6.

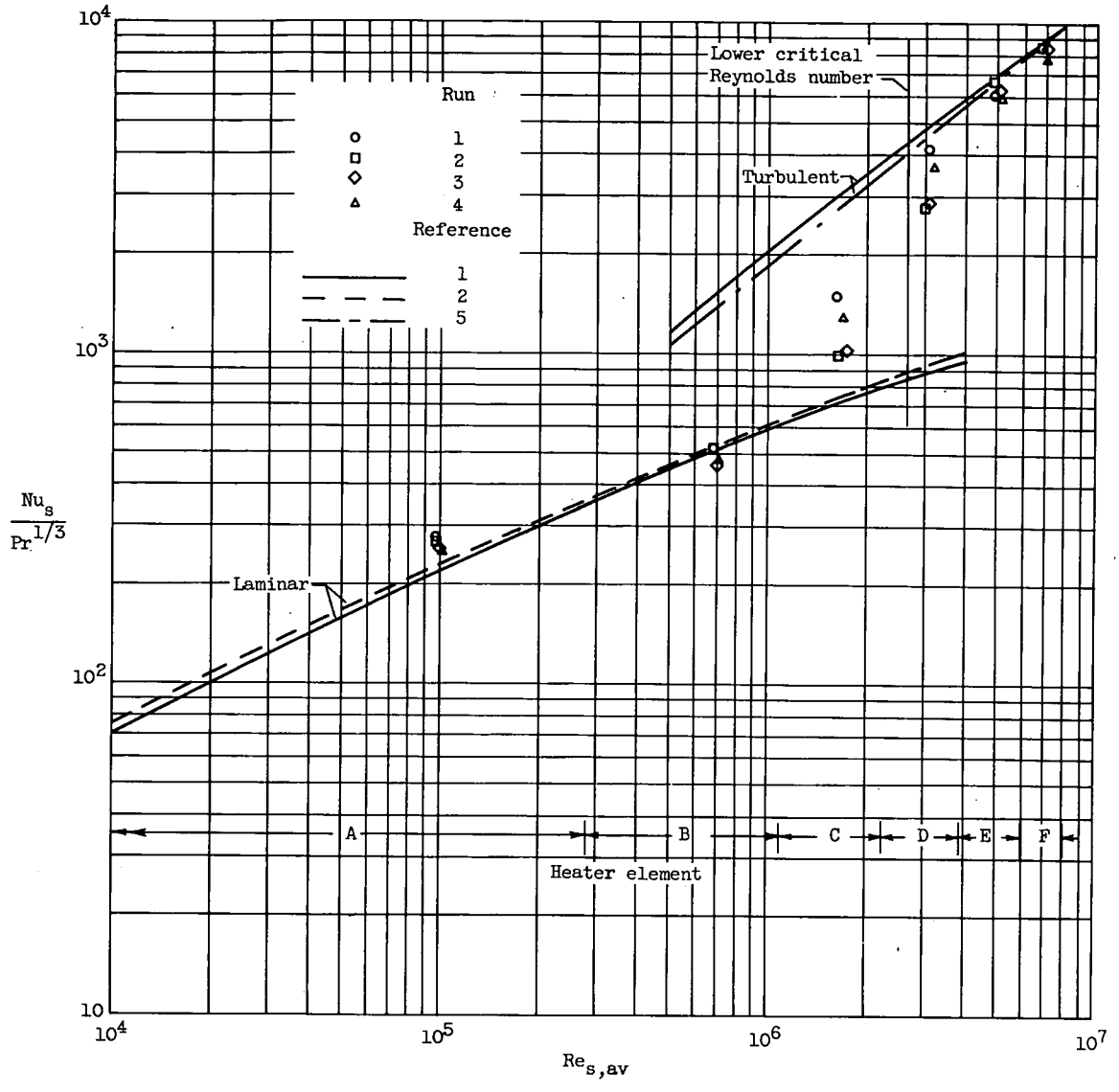

(a) Stationary spinner at angle of attack of 0°, free-stream velocity of 237 knots, air total temperature of 0° F, surface temperature of 100° F, and free-stream Reynolds number of 5×10^6.

Figure 8. - Heat transfer obtained at several rotational speeds and angles of attack for spinner with uniform surface temperature.

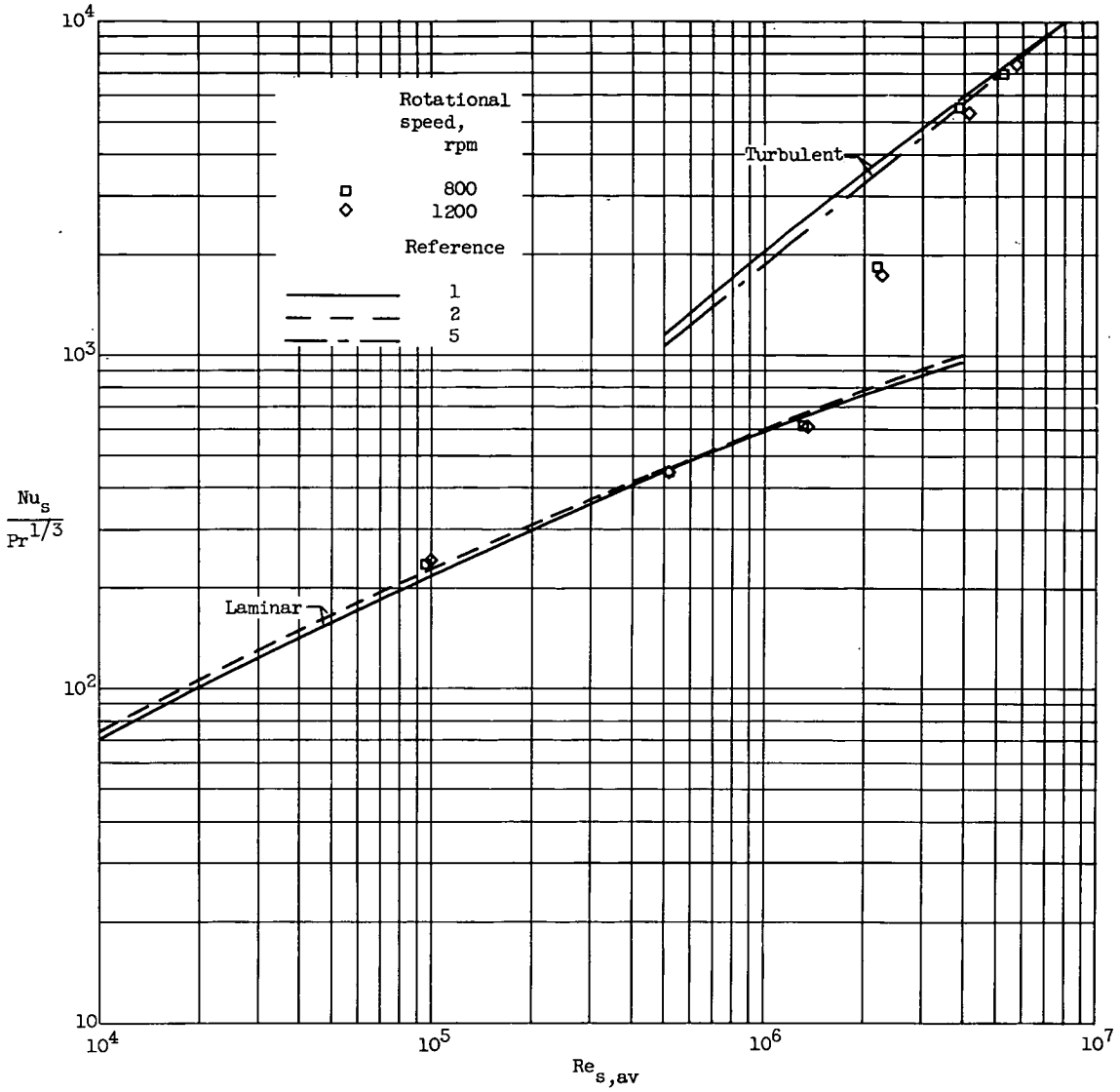

(b) Rotating spinner at angle of attack of 3°, free-stream velocity of 168 knots, air total temperature of 3° F, surface temperature of 200° F, and free-stream Reynolds number of 3.6×10^6.

Figure 8. - Continued. Heat transfer obtained at several rotational speeds and angles of attack for spinner with uniform surface temperature.

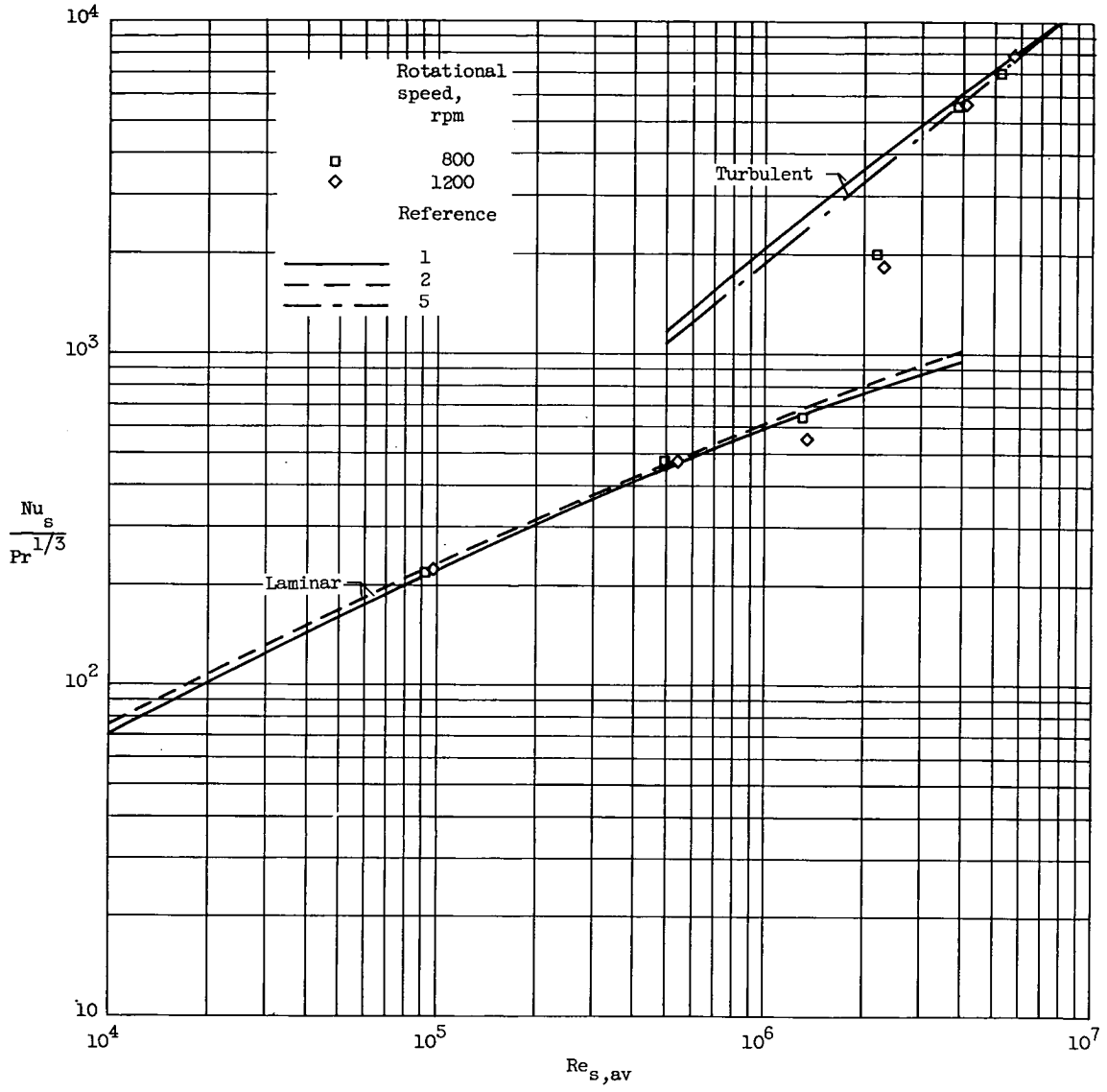

(c) Rotating spinner at angle of attack of 6°, free-stream velocity of 171 knots, air total temperature of 2° F, surface temperature of 200° F, and free-stream Reynolds number of 3.6×10^6.

Figure 8. - Concluded. Heat transfer obtained at several rotational speeds and angles of attack for spinner with uniform surface temperature.

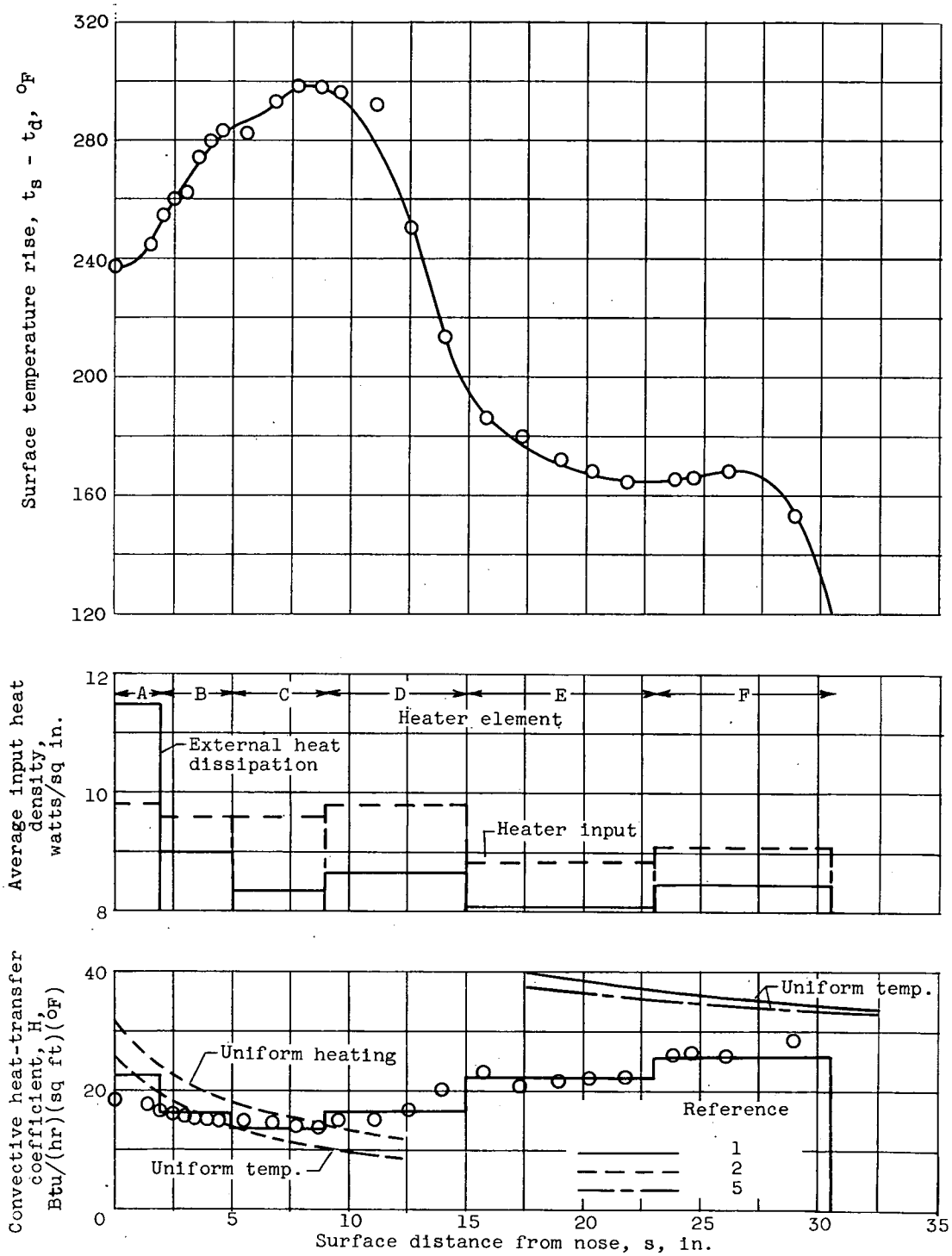

Figure 9. - Distribution of surface temperature, heater power density, and convective heat-transfer coefficient for stationary spinner with uniform heat input. Free-stream velocity, 156 knots; air total temperature, 0° F; angle of attack, 0°.

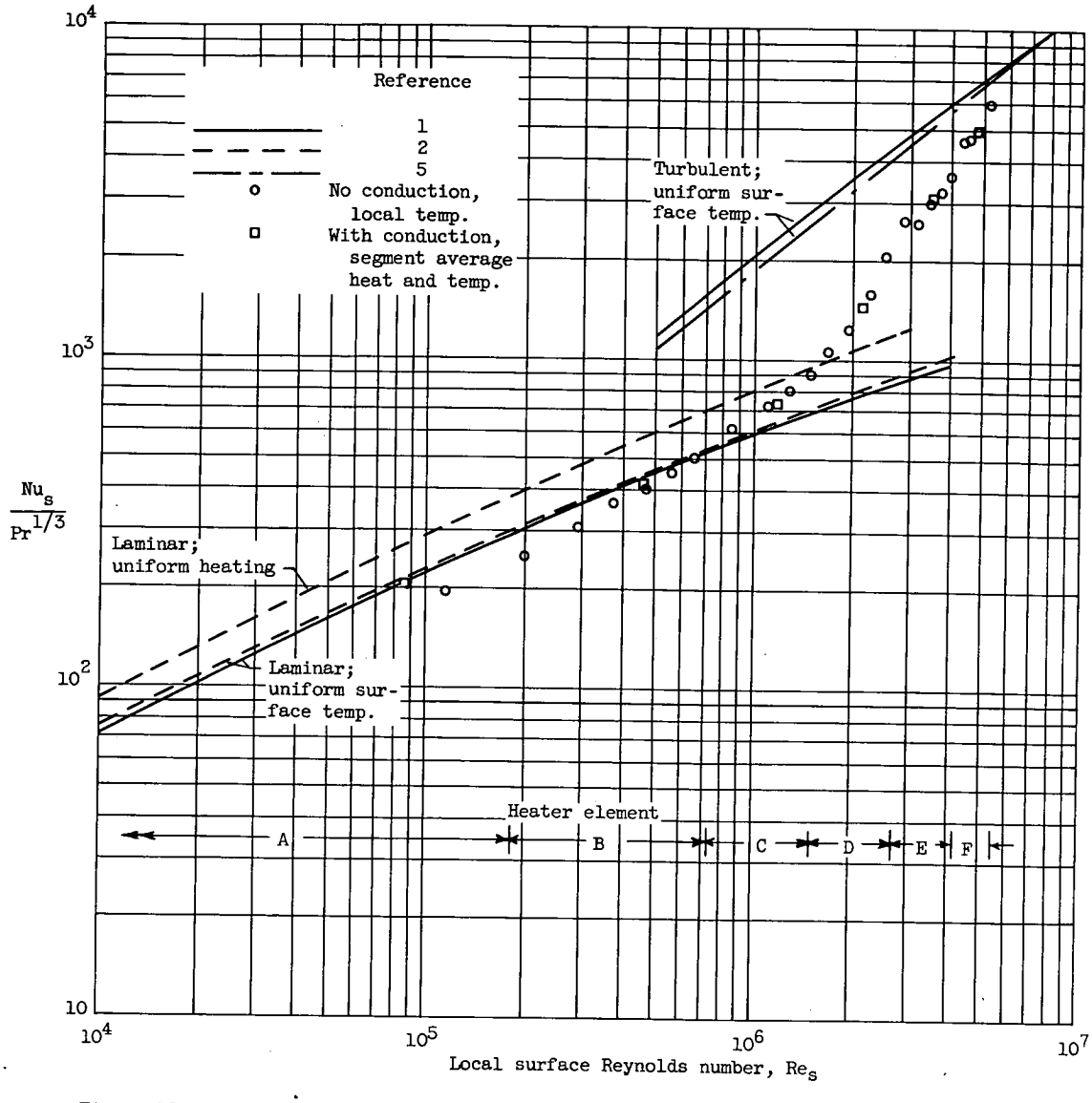

Figure 10. - Correlation of experimental and theoretical heat transfer for stationary spinner having uniform heat input. Free-stream velocity, 156 knots; air total temperature, 0° F; angle of attack, 0°.

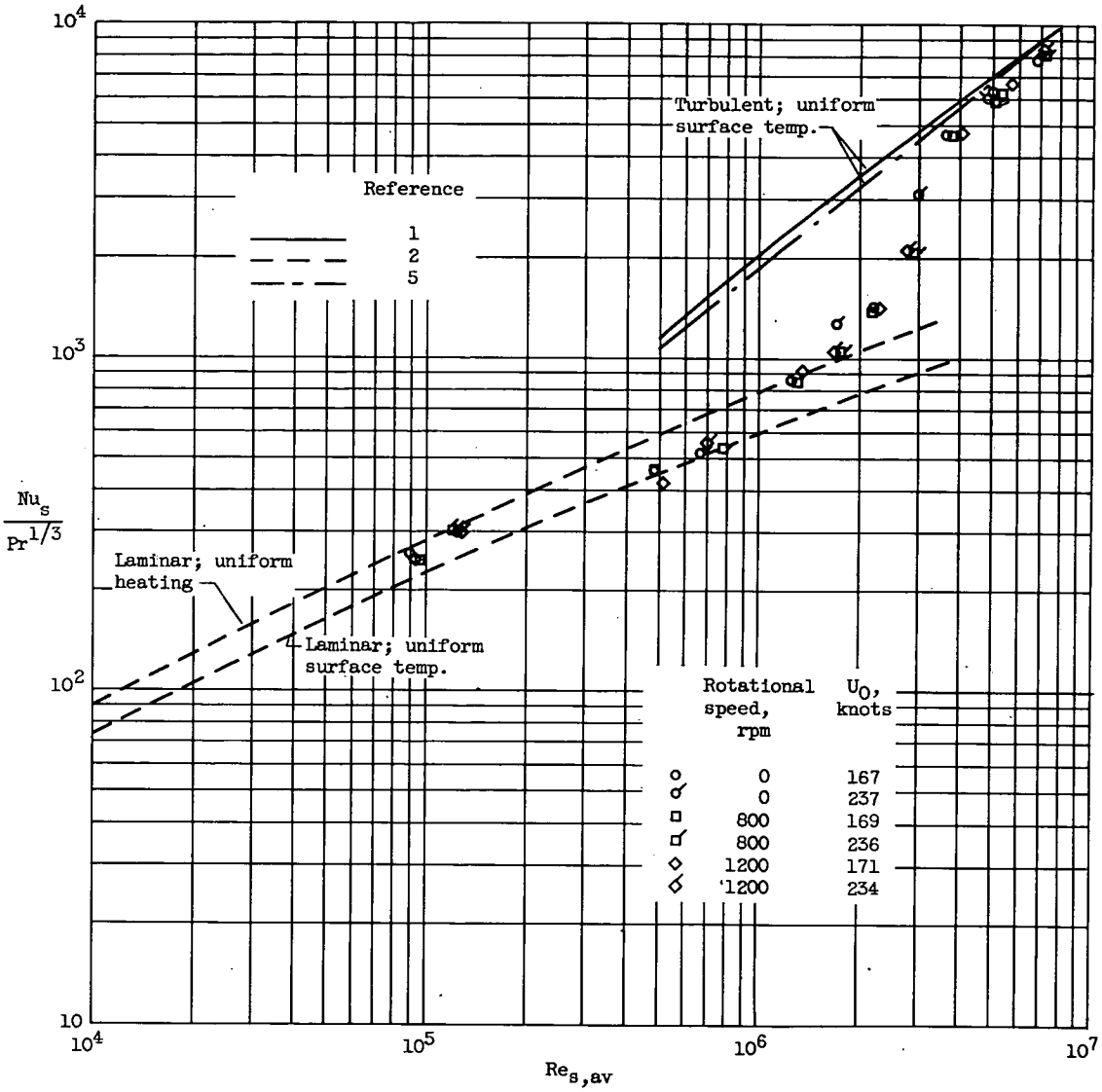

(a) Angle of attack, 0°.

Figure 11. - Comparison of heat-transfer data obtained for stationary and rotating spinner having uniform heat input at average air total temperature of -2° F.

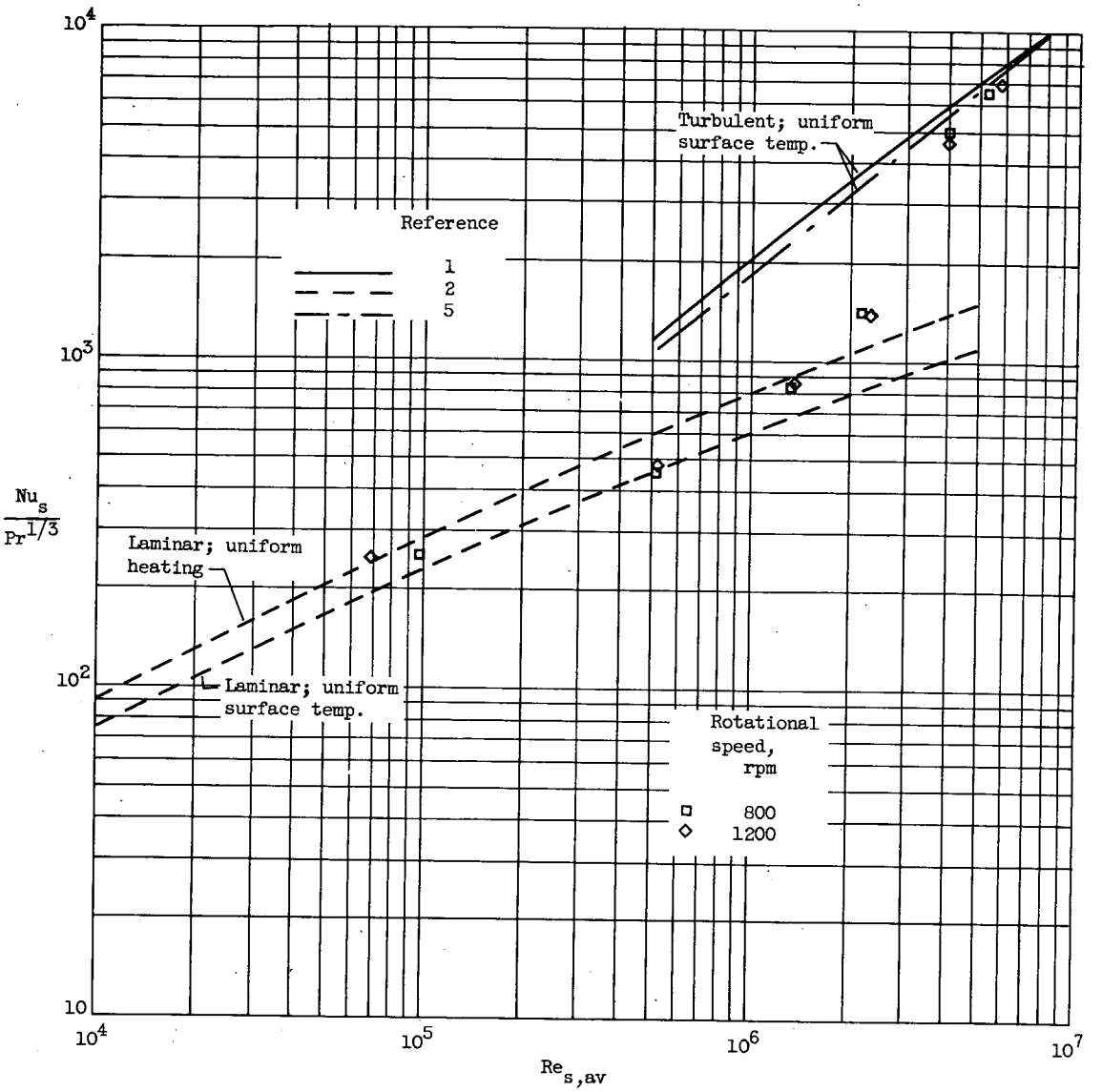

(b) Angle of attack, 3°; free-stream velocity, 169 knots; air total temperature, 2° F.

Figure 11. - Continued. Comparison of heat-transfer data obtained for stationary and rotating spinner having uniform heat input at average air total temperature of -2° F.

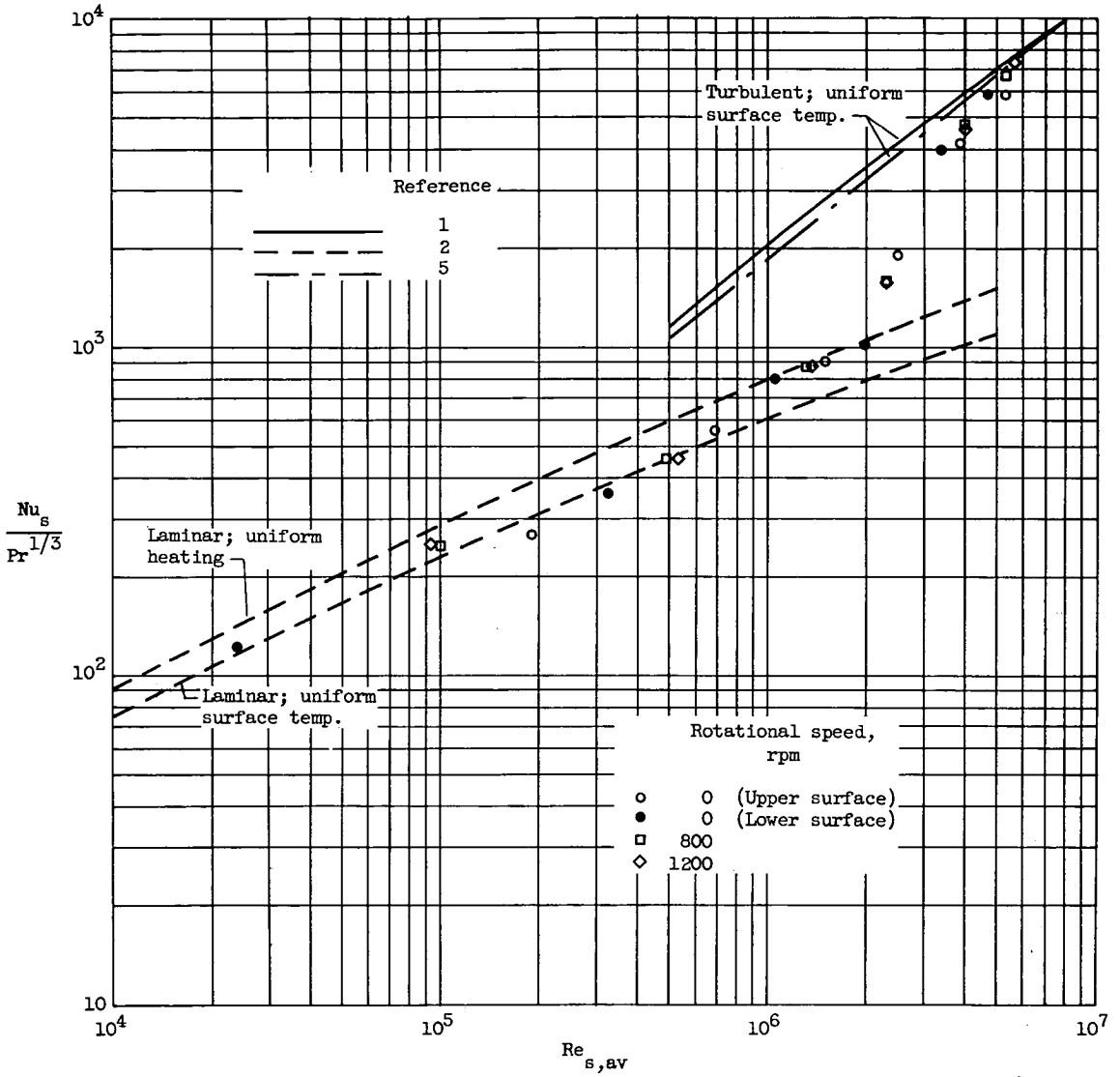

(c) Angle of attack, 6°; free-stream velocity, 170 knots; air total temperature, 2° F.

Figure 11. - Concluded. Comparison of heat-transfer data obtained for stationary and rotating spinner having uniform heat input at average air total temperature of -2° F.

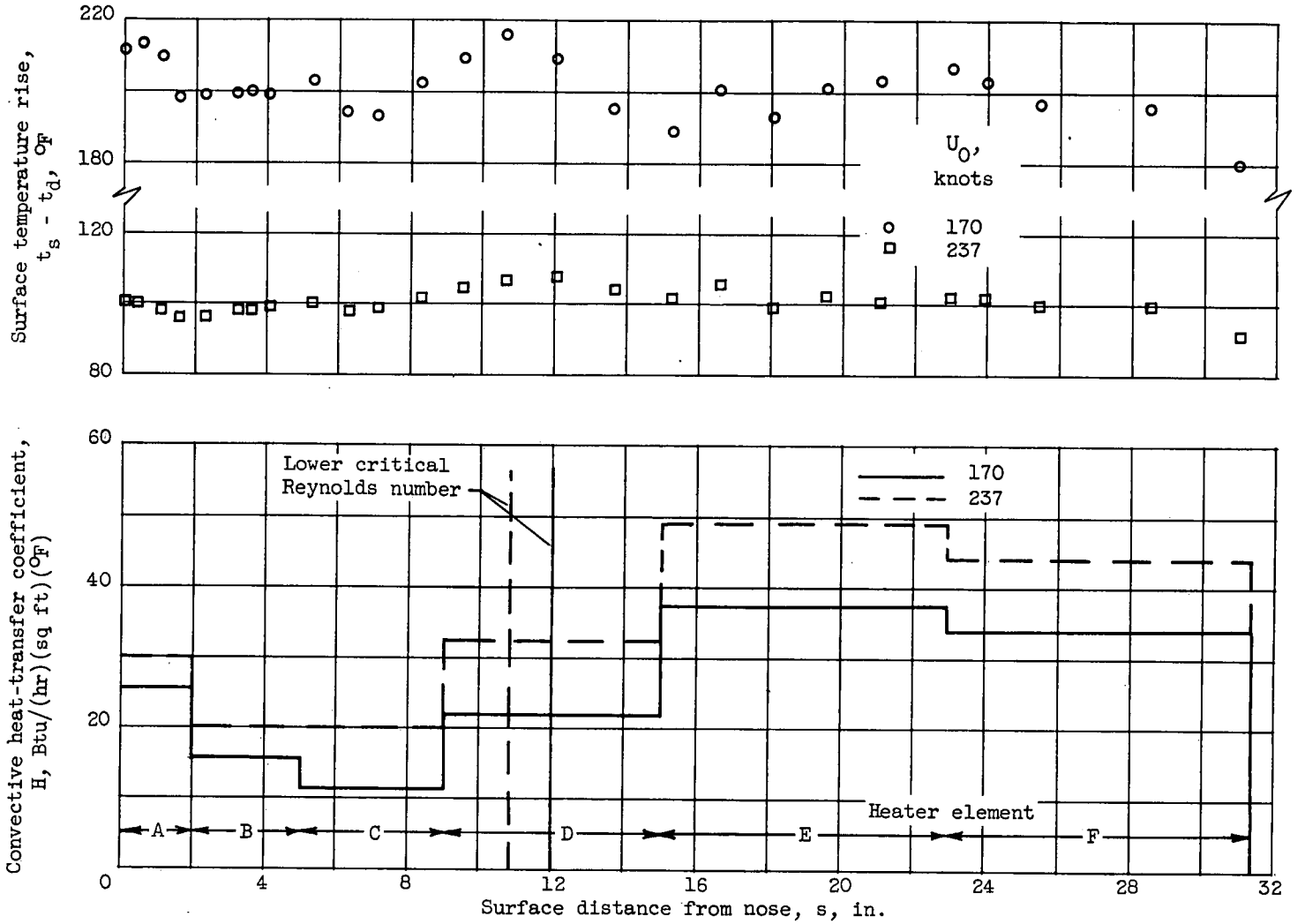

(a) Uniform surface temperature distribution.

Figure 12. - Comparison of heat transfer and surface temperature rise obtained at two free-stream velocities for stationary spinner at air total temperature of 2° F and angle of attack of 0°.

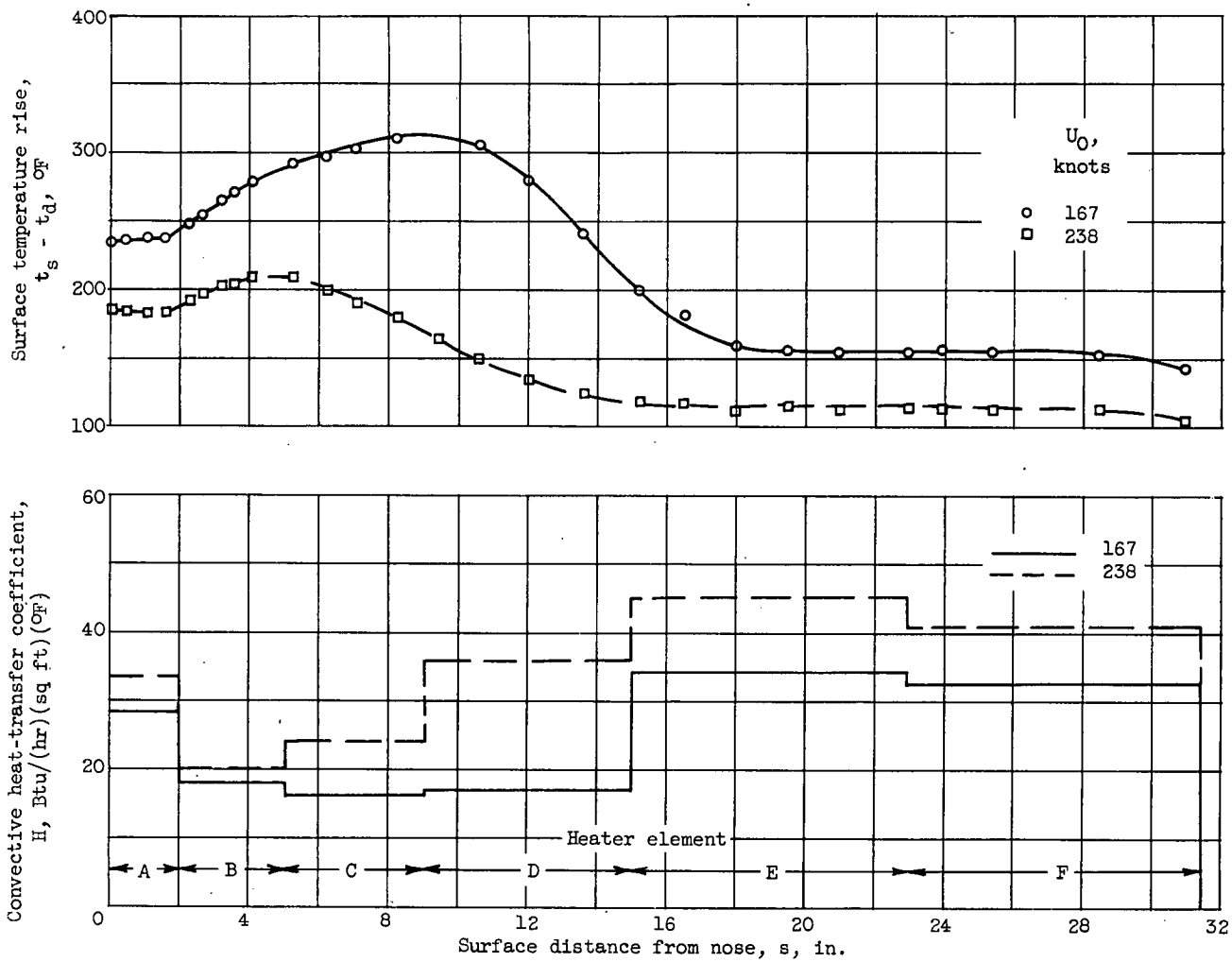

(b) Uniform input heat density of approximately 10 watts per square inch.

Figure 12. - Concluded. Comparison of heat transfer and surface temperature rise obtained at two free-stream velocities for stationary spinner at air total temperature of 2° F and angle of attack of 0°.

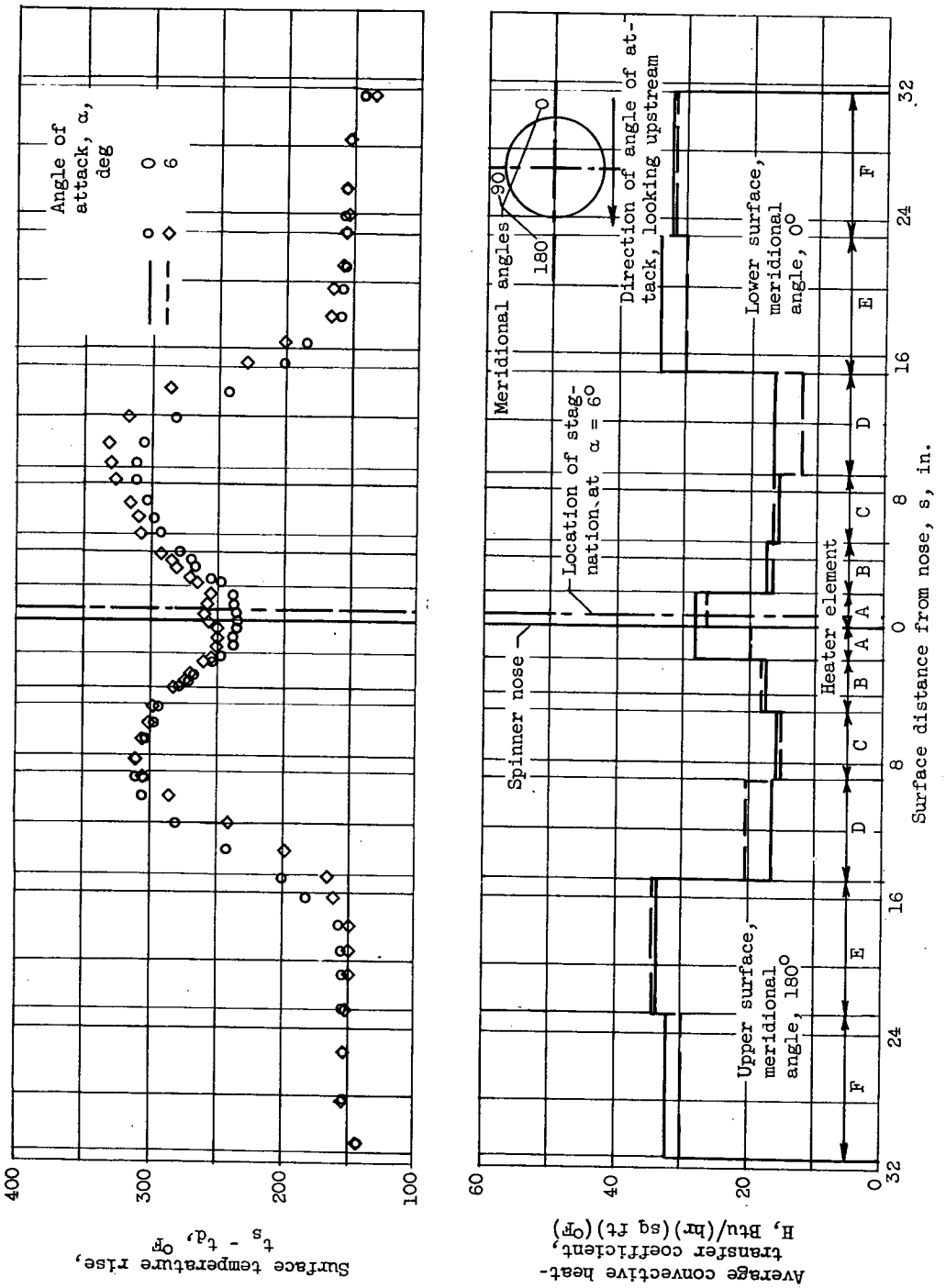

(a) Two angles of attack at two meridional locations.

Figure 13. - Comparison of heat transfer and surface temperature rise obtained at angle of attack for stationary spinner. Uniform heat input density, approximately 10 watts per square inch; free-stream velocity, 167 knots; air total temperature, 2° F.

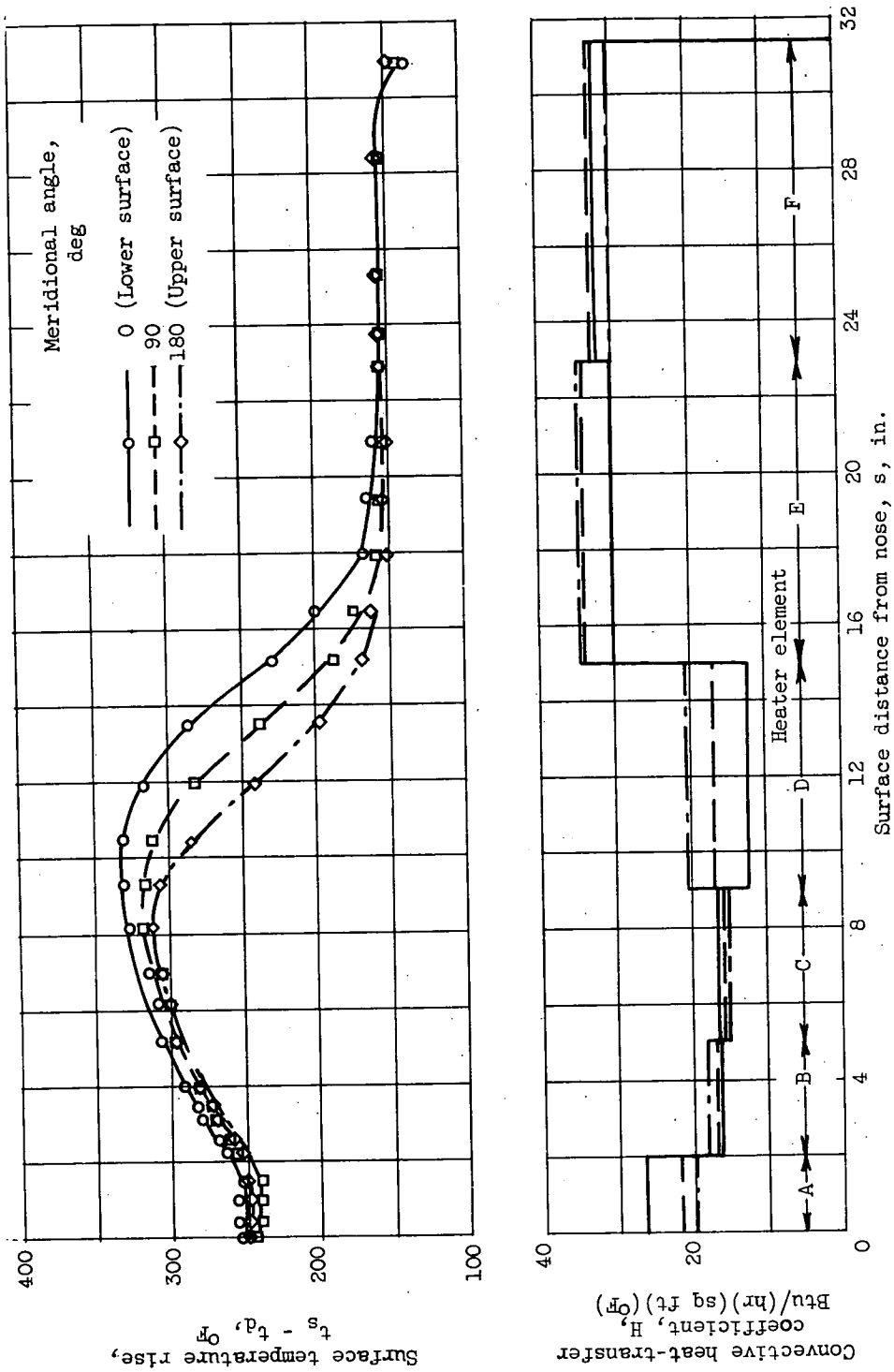

(b) Three meridional locations at 6° angle of attack.

Figure 13. - Concluded. Comparison of heat transfer and surface temperature rise obtained at angle of attack for stationary spinner. Uniform heat input density, approximately 10 watts per square inch; free-stream velocity, 167 knots; air total temperature, 2° F.

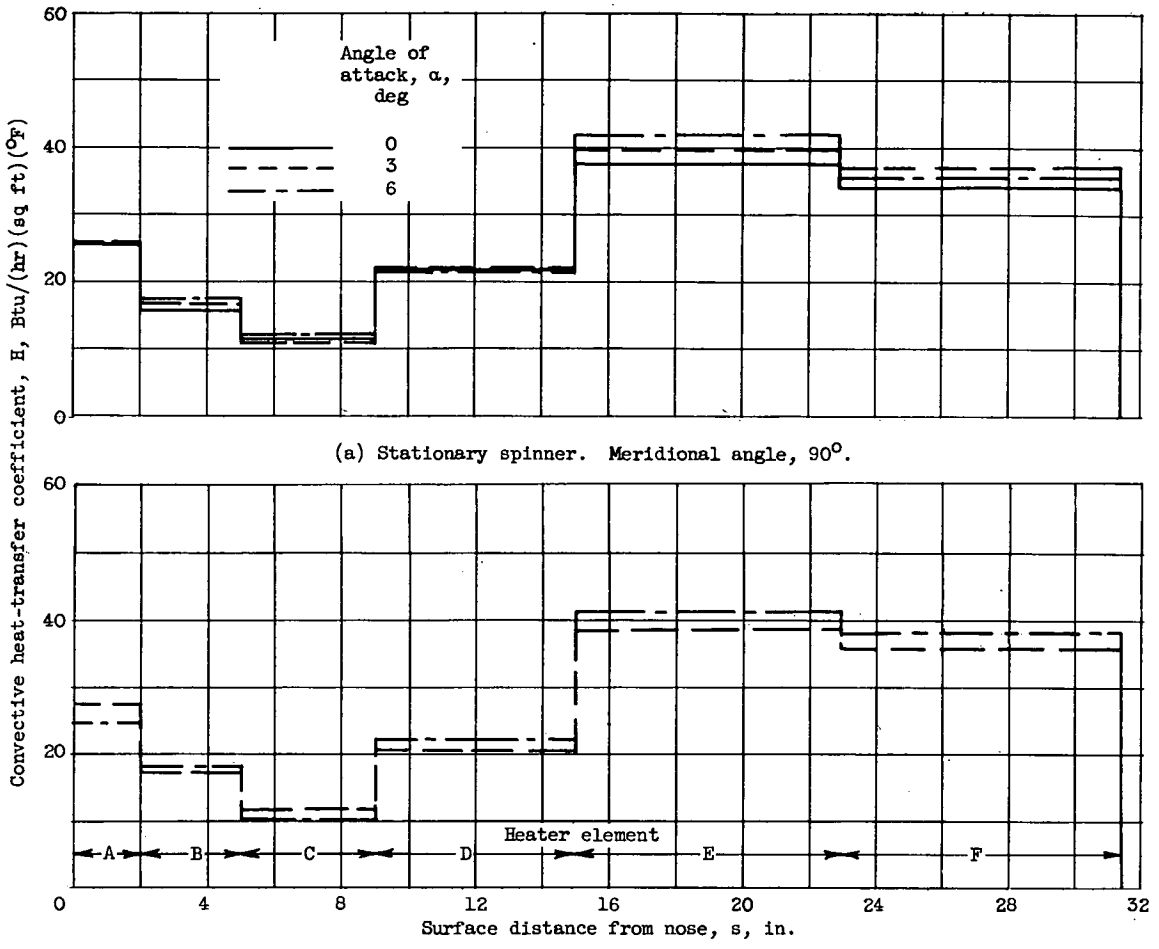

(a) Stationary spinner. Meridional angle, 90°.

(b) Rotational speed, 1200 rpm.

Figure 14. - Variation of heat transfer with rotational speed and angle of attack for spinner with uniform surface temperature distribution. Free-stream velocity, 170 knots; air total temperature, 2° F.

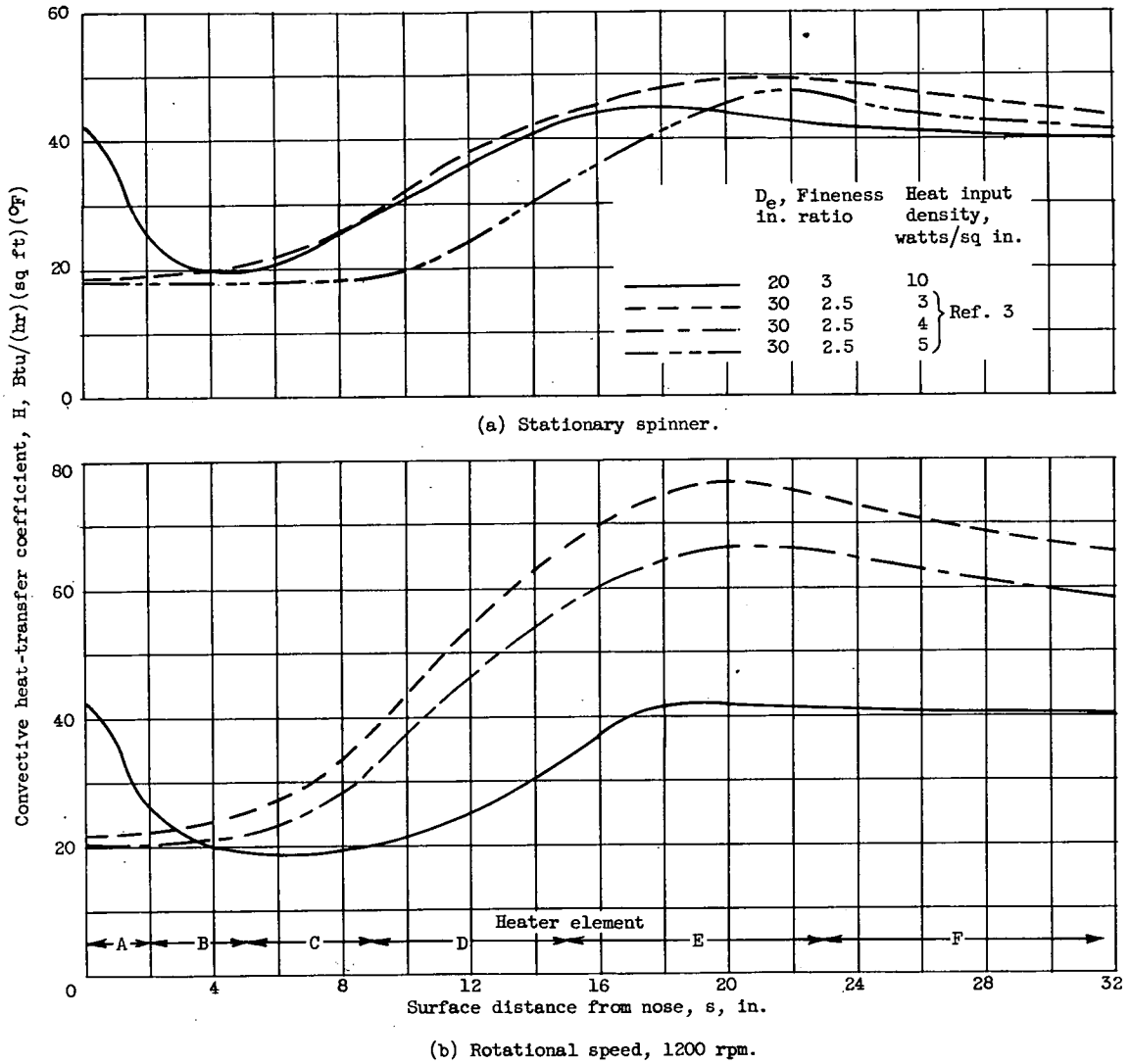

(a) Stationary spinner.

(b) Rotational speed, 1200 rpm.

Figure 15. - Comparison of convective heat-transfer coefficients for two spinners at 0° angle of attack and uniform input heat density. Free-stream velocity, 237 knots; air total temperature, 0° F.

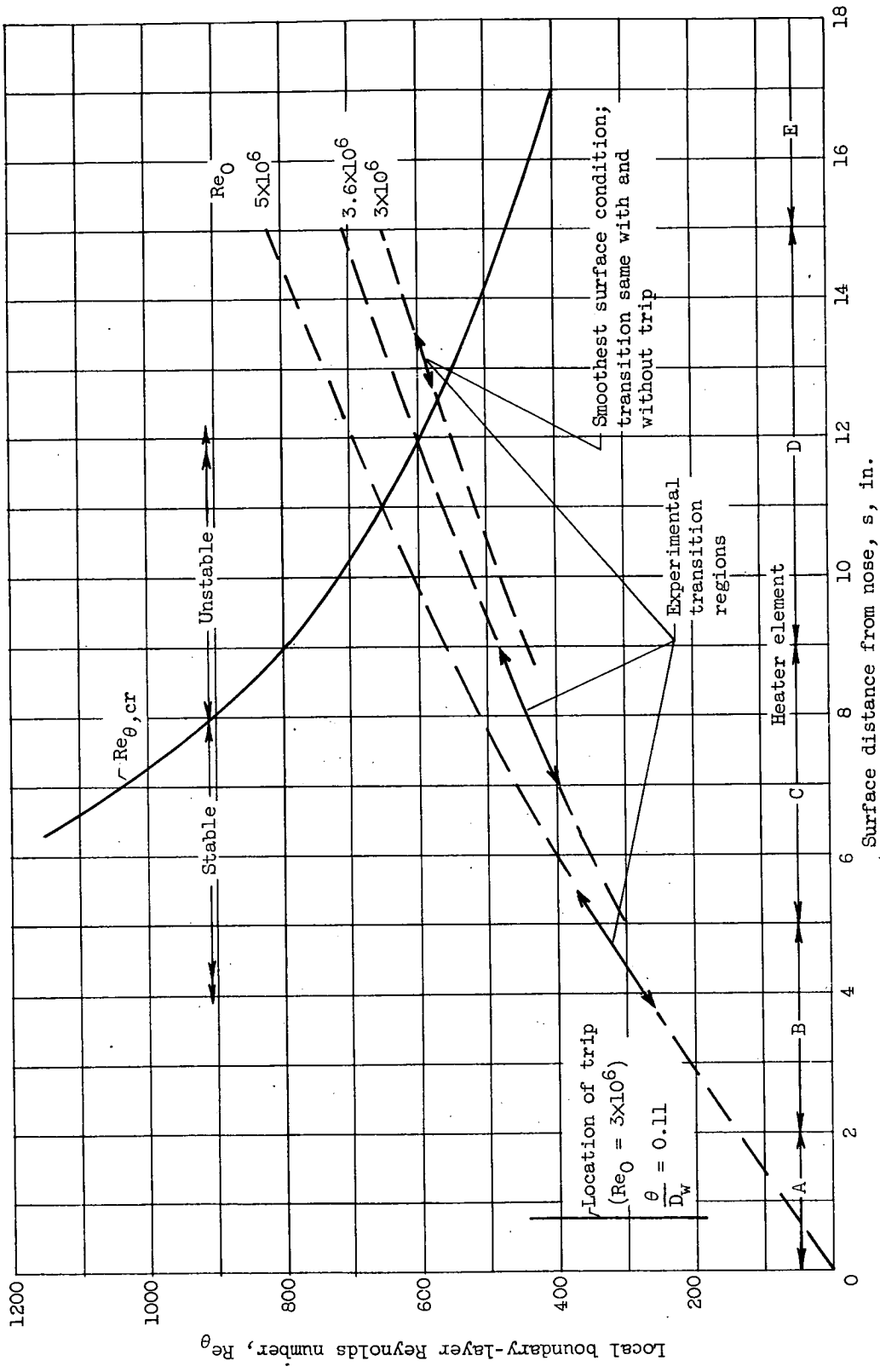

Figure 16. - Comparison of experimental transition with calculated stability limits. Stationary spinner, uniform surface temperature, and 0° angle of attack.

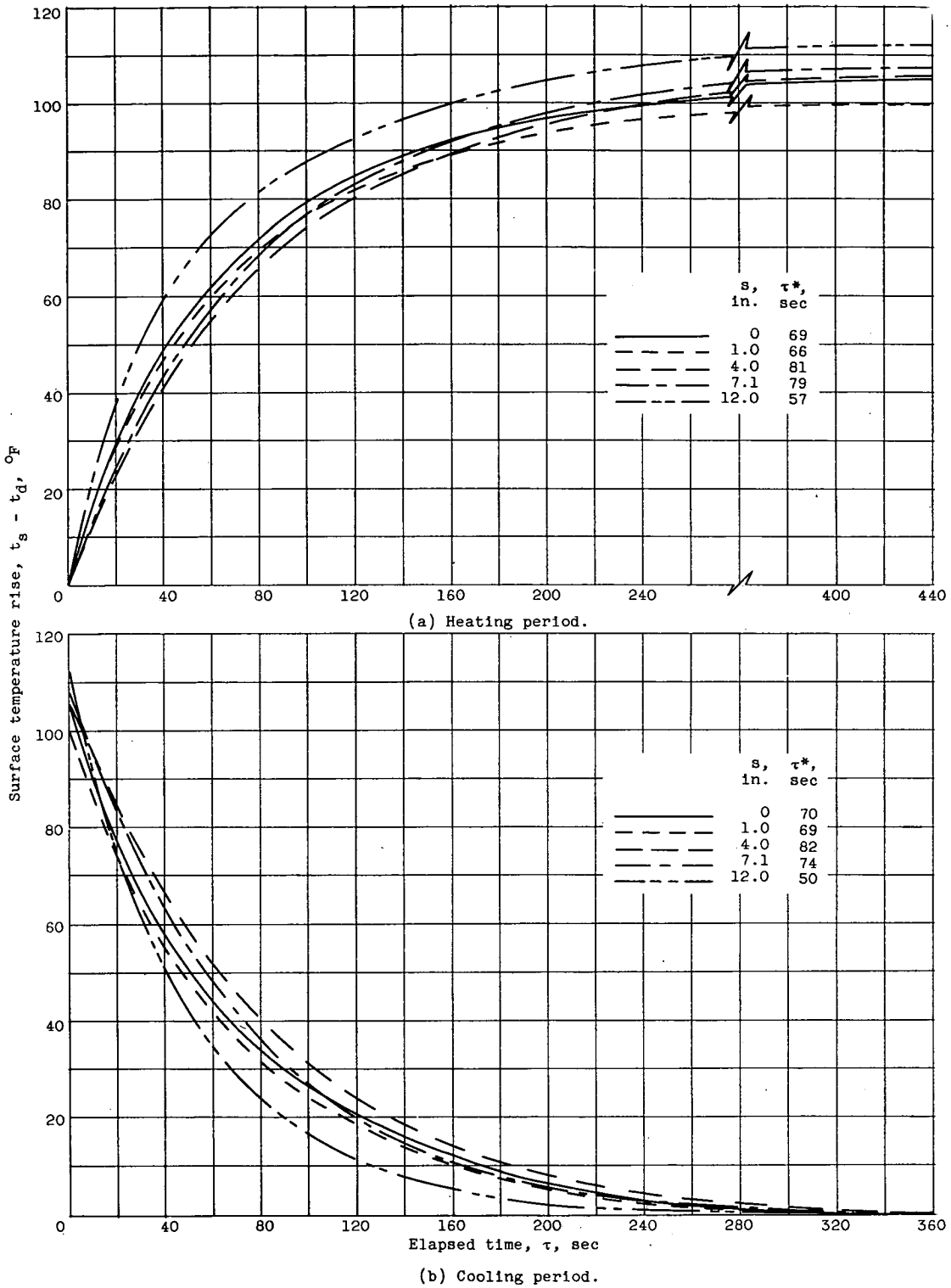

Figure 17. - Variation of surface temperature with elapsed time for stationary spinner. Angle of attack, 0°; free-stream velocity, 240 knots; air total temperature, 2° F.

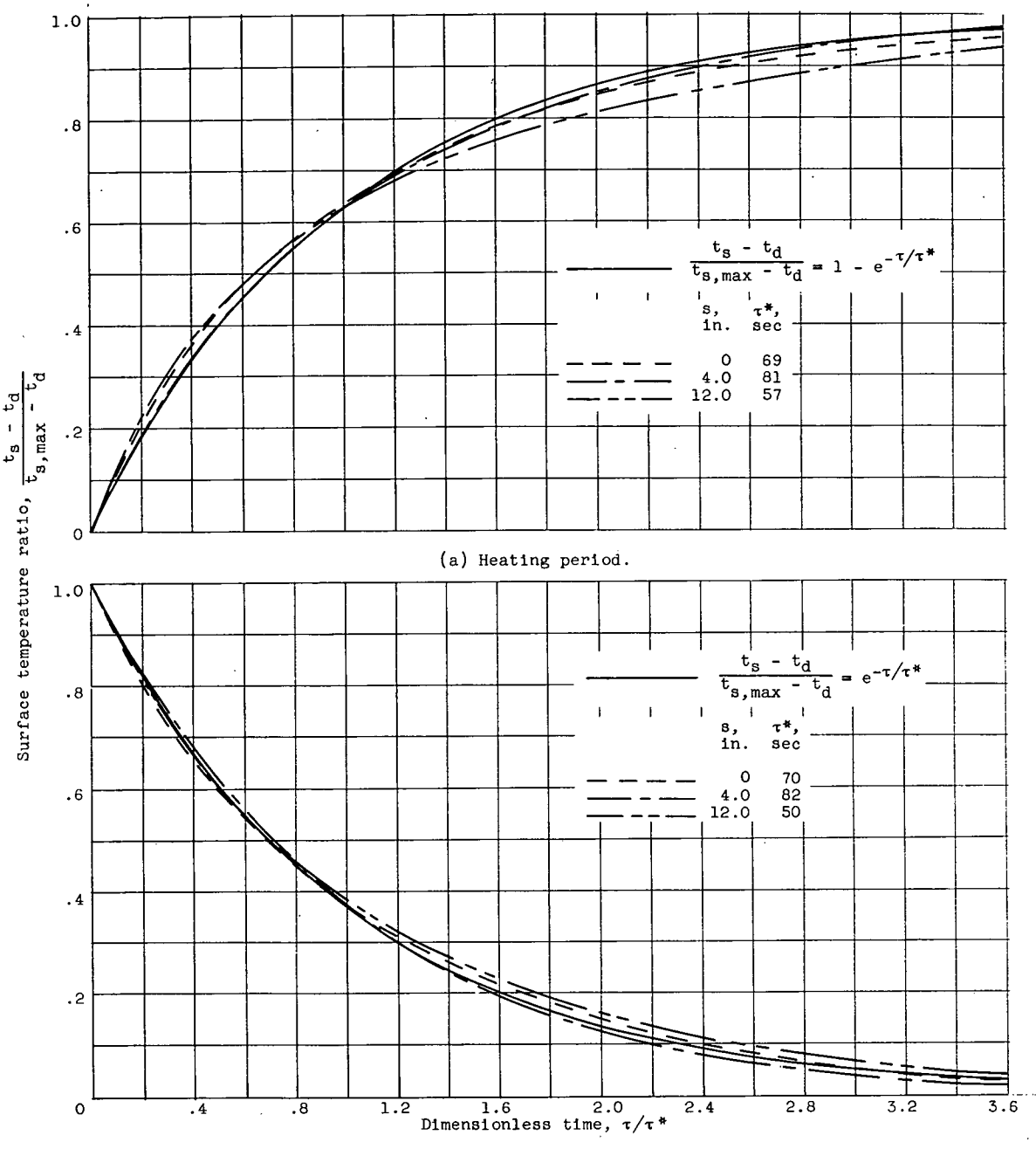

(a) Heating period.

(b) Cooling period.

Figure 18. - Surface temperature variation with time for stationary spinner. Angle of attack, 0°; free-stream velocity, 240 knots; air total temperature, 2° F.